Motor Learning Promotes Remyelination via New and Surviving Oligodendrocytes

Clara M. Bacmeister[1,*], **Helena J. Barr**[1,*], **Crystal R. McClain**[1,*], **Michael A. Thornton**[1], **Dailey Nettles**[1,2,3], **Cristin G. Welle**[2,3], **Ethan G. Hughes**[1,4]

[1]Department of Cell and Developmental Biology; University of Colorado School of Medicine; Aurora; Colorado; USA.

[2]Department of Neurosurgery; University of Colorado School of Medicine; Aurora; Colorado; USA.

[3]Department of Physiology and Biophysics; University of Colorado School of Medicine; Aurora; Colorado; USA.

Abstract

Oligodendrocyte loss in neurological disease leaves axons vulnerable to damage and degeneration, and activity-dependent myelination may represent an endogenous mechanism to improve remyelination following injury. Here, we report that while learning a forelimb reach task transiently suppresses oligodendrogenesis, it subsequently increases OPC differentiation, oligodendrocyte generation, and myelin sheath remodeling in the forelimb motor cortex. Immediately followingdemyelination, neurons exhibit hyperexcitability, learning is impaired, and behavioral intervention provides no benefit to remyelination. However, partial remyelination restores neuronal and behavioral function allowing learning to enhance oligodendrogenesis, remyelination of denuded axons, and the ability of surviving oligodendrocytes to generate new myelinsheaths. Previously considered controversial, we show that sheath generation by mature oligodendrocytes is not only possible but also increases myelin pattern preservation following demyelination, presenting a new target for therapeutic interventions. Together, our findings demonstrate that precisely-timed motor learning improves recovery from demyelinating injury via enhanced remyelination from new and surviving oligodendrocytes.

---

[4]Corresponding author. ethan.hughes@cuanschutz.edu.
[*]These authors contributed equally to this work.

Introduction

Oligodendrocytes, the myelin-forming cells of the central nervous system (CNS), enhance the propagation of action potentials and support neuronal and axonal integrity through metabolic coupling. Injury to oligodendrocytes critically affects axonal health and is associated with significant neurologic disability in patients with multiple sclerosis (MS)[1]. While a growing number of immunotherapies decrease the frequency of MS attacks, they do not fully prevent axonal degeneration nor the accumulation of disability[2]. Oligodendrocyte precursor cells (OPCs) can generate new oligodendrocytes with the capacity to remyelinate denuded axons, which can restore neuronal function[3,4]. However, remyelination is typically incomplete in patients with MS[5] and approaches to increase myelin repair remain limited[6]. Interestingly, recent studies show oligodendrocyte turnover varies considerably across MS patients and posit a controversial role for pre-existing oligodendrocytes in remyelination[7,8]. While current dogma maintains that mature oligodendrocytes do not participate in remyelination[9], recent evidence suggests that myelinating oligodendrocytes may make new myelin sheaths in large animal models of demyelinating injury[10]. Furthermore, neuronal activity can modify myelin sheaths via adjustments to internode length and thickness, raising the possibility that mature oligodendrocytes can alter their myelination in an activity-dependent manner[11]. Together, these findings suggest the existence of endogenous mechanisms that may modulate myelin repair by new and surviving oligodendrocytes following demyelinating injury.

Motor learning drives white matter changes in humans and rodents in part by eliciting the proliferation and differentiation of OPCs in the adult CNS[12,13] similar to OPC responses to demyelinating injuries[4], yet it remains unclear whether learning during demyelination has synergistic or antagonistic effects. Behavioral interventions are increasingly personalizable in clinical settings and are used to ameliorate motor function in myelin disease patients[14]. Optimizing the modality and timing of behavioral interventions may allow endogenous mechanisms of myelin plasticity to act in synchrony and drive more robust remyelination following injury.

Through longitudinal *in vivo* two-photon imaging of oligodendrocyte lineage cells and individual myelin sheaths, we defined the complex dynamics between motor skill acquisition and oligodendroglia in the motor cortex. We studied this in both developmental and remyelinating contexts using the cuprizone-mediated demyelination model, which results in ongoing oligodendrocyte death and regeneration similar to cortical lesions in MS patients[15] without the confound of autoimmunity. We found that motor learning, when properly timed, could enhance oligodendrogenesis after injury and recruit mature oligodendrocytes to participate in remyelination through the generation of new myelin sheaths.

Results

Forelimb reach training dynamically modulates oligodendrocyte lineage cells and myelination

Previous assessments using cell lineage tracing and stage-specific markers[16,17] indicate that motor learning rapidly increases adult oligodendrogenesis, yet the dynamics of activity-dependent myelination remain unclear due to incomplete labeling of differentiating OPC populations and inter-individual variability in cross-sectional approaches. To determine the dynamics of oligodendrocytes, myelin, and OPCs during learning, we used longitudinal two-photon *in vivo* imaging in the forelimb-region of motor cortex throughout learning and rehearsal of a skilled, single-pellet contralateral forelimb reach task[18] (Fig. 1a,b; Extended Data Fig. 1; Supplementary Video 1). We used transgenic mice that express EGFP in all cortical myelinating oligodendrocytes and myelin sheaths[19] (*MOBP-EGFP*, Fig. 1c; Supplementary Video 2) to examine the effects of learning on oligodendrogenesis and pre-existing myelin sheath remodeling in healthy mice. Long-term *in vivo* imaging of layers I-III allowed us to track ~100 oligodendrocytes and their myelin sheaths over the course of 2–3 months per mouse. Immunohistochemistry, *in vivo* SCoRe imaging, and semi-automated tracing confirmed that EGFP in *MOBP-EGFP* transgenic mice faithfully reflects the presence and length of myelin sheaths and allows morphological reconstruction of individual oligodendrocytes (Simple Neurite Tracer[20]; Extended Data Fig. 2; Supplementary Video 3). Assuming a range of 45±4 sheaths per cortical oligodendrocyte[19], our average sampling was 67–74% of an individual oligodendrocyte arbor.

To separate the effects of motor learning from performance, we performed *in vivo* imaging during initial training ("learning"; 7 days of 20-minute sessions), or performance of the task one month post-training ("rehearsal"; 5 days of 20-minute sessions for 3 weeks; Fig. 1b). Of all trained mice, 93% were able to learn the task, and both learning and rehearsal of the task resulted in skill refinement (Extended Data Fig. 1). We trained mice between 2–3 months old, when oligodendrogenesis is ongoing (Extended Data Fig. 3).

We found that learning the reach task transiently decreased and subsequently increased the rate of oligodendrogenesis in forelimb motor cortex (Fig. 1d,e). During learning, oligodendrogenesis rate decreased by ~75% relative to age-matched controls (0.14±0.03% vs. 0.58±0.08%, respectively; rate refers to the % increase in cells over the number of days elapsed). Suppression of oligodendrogenesis was restricted to the training period and was not mediated by the effects of handling (all mice were handled equally) or training-related diet restriction (Extended Data Fig. 3). Immediately following learning, oligodendrogenesis rate increased resulting in an almost two-fold greater rate of oligodendrogenesis relative to untrained controls (0.77±0.19% vs. 0.40±0.04, respectively; Fig. 1e), and remained elevated for 3 weeks (Extended Data Fig. 3). Proficiency in the reach task predicted the magnitude of oligodendrogenesis rate increase following learning (Extended Data Fig. 3). In contrast, rehearsal of the task did not alter oligodendrogenesis rates relative to controls, and the post-learning burst in oligodendrogenesis eventually tapered off (Fig. 1f, Extended Data Fig. 3). Overall, mice that had been trained (both "learning" and "rehearsal") had higher maximum rates of oligodendrogenesis than untrained mice (Extended Data Fig. 3). Only layer I of

forelimb motor cortex demonstrated consistent changes in post-learning oligodendrogenesis rate (Fig. 1g), where motor learning strengthens horizontal connections between neurons[21]. Oligodendrogenesis rate in layers II/III was variable across mice.

Next, we examined remodeling of pre-existing myelin sheaths throughout learning. Under normal physiological conditions, we found a small number of myelin sheaths exhibited dynamic length changes, similar to previous descriptions in young adult mice[22] (14.7±1.71%; Fig. 1h,i; Supplementary Video 4,5). One week post-learning, the proportion of dynamic pre-existing myelin sheaths increased in learning mice relative to controls (43.46±7.82% vs. 14.74±1.71%). Learning increased both the proportion of sheaths that underwent retraction and the distance these sheaths retracted compared to untrained mice (Fig. 1i,j). Learning also modulated the timing of sheath remodeling; growing sheaths ceased to lengthen at the onset of learning, while learning induced the retraction of previously stable sheaths (Fig. 1k). We found no evidence that new myelin sheaths were generated by pre-existing oligodendrocytes in untrained or learning mice.

To further characterize how motor skill learning modulates the generation of new mature oligodendrocytes, we used longitudinal *in vivo* two-photon imaging of transgenic mice that express membrane-anchored EGFP in oligodendrocyte precursor cells (OPCs; *NG2-mEGFP*[23]) to track OPC migration, proliferation, differentiation, and death in forelimb motor cortex over 5 weeks, beginning 1 week prior to forelimb reach training (Fig. 2a,b). Similar to oligodendrogenesis, learning induced a two-fold increase in the rate of OPC differentiation in the week following learning (Fig. 2c, 0.59±0.10% during learning vs. 1.23±0.19% post-learning), yet OPC differentiation rate was unaffected during reach training. Neither the rates of proliferation nor death differed significantly across the five weeks (Fig. 2d,e). However, 5/5 mice displayed a reduction in proliferation rate (~50%) during learning relative to baseline (Extended Data Fig. 3). Our previous work indicated that a majority of adult OPC differentiation events occur via direct differentiation rather than asymmetric cell division[23]. In line with these findings, we found that only 10.91±3.77% of differentiating OPCs had previously proliferated during the 5 weeks of observation. The proportion of asymmetric differentiation events was unaffected by motor learning (Fig. 2a,f,g). To assess whether the increase in OPC differentiation following motor learning was due to parenchymal OPCs or precursors recruited from nearby brain regions or germinal zones, we tracked OPCs that migrated into the imaging volume (Extended Data Fig. 3). Migration into the field was rare, with 4.68±0.96% of the baseline number of OPCs migrating in and 2.73±0.36% migrating out and was not altered by learning. Only 3.57±1.49% of the total proliferation events and 0.70±0.30% of the total differentiation events occurred in cells that migrated into the imaging volume. These data indicate that parenchymal OPCs residing in motor cortex directly differentiated following acquisition of the reach task.

Demyelination results in incomplete oligodendrocyte replacement, changes to the pattern of myelination, and functional deficits in motor cortex

Gray matter lesions in patients with MS contain both dying and newly forming oligodendrocytes[15], a feature that has complicated the interpretation of remyelination in

humans and animal models of MS[24]. To visualize the dynamics of myelin loss and repair, we used longitudinal two-photon *in vivo* imaging during cuprizone-mediated demyelination (Fig. 3a; Supplementary Video 6). We fed 10-week-old congenic *MOBP-EGFP* mice a 0.2% cuprizone diet for three weeks to induce oligodendrocyte death (~90% in forelimb motor cortex, Fig. 3a-h), and confirmed that *in vivo* two-photon analysis of *MOBP-EGFP* mice is a reliable measure of oligodendrocyte and myelin sheath loss with SCoRe and immunohistochemistry (Extended Data Fig. 4). In contrast to the loss of myelin and mature oligodendrocytes, the number of cortical OPCs was unchanged following cuprizone administration relative to age-matched controls (Extended Data Fig. 4, 138.63±19.75 cells/mm^2 vs. 179.11±14.99 cells/mm^2, respectively), similar to recently published studies[25].

Oligodendrocyte loss occurred evenly across cortical depths (Extended Data Fig. 5), leaving a small number of oligodendrocytes and myelin intact (12.94±3.10%, "surviving" oligodendrocytes; Fig. 3b,c). Cuprizone treatment suppressed oligodendrogenesis, and 85% of the few cells generated during cuprizone administration died within 3 weeks (Extended Data Fig. 5). Oligodendrocyte death followed a biphasic model of myelin loss (1.53±1.27 days before cuprizone cessation) followed by cell body loss (7.26±1.22 days post-cuprizone; Fig. 3d,e; Supplementary Video 7), similar to previous descriptions of demyelination occurring via a "dying-back" process[26]. Oligodendrocyte loss plateaued approximately fifteen days following the cessation of cuprizone administration (Fig. 3f). Cuprizone diet removal induced a robust oligodendrogenesis response that was proportional to the extent of oligodendrocyte loss and that plateaued at approximately three weeks (Fig. 3f,g; Extended Data Fig. 5). The cortical distribution of newly generated oligodendrocytes was comparable in remyelinating and healthy conditions. Maximum oligodendrogenesis rates during remyelination were six times greater than in healthy untrained mice (5.95±0.38% vs. 0.99±0.69%) and almost four times greater than in healthy trained mice (5.95±0.38% vs. 1.60±0.64%; Extended Data Fig. 5).

To further characterize the oligodendrogenesis response, we tracked mice up to 60 days after cuprizone cessation. Due to the oral uptake of cuprizone, there was inter-mouse variation in the extent of demyelination, and consequently, remyelination (Extended Data Fig. 5). We therefore quantified oligodendrocytes generated during remyelination as a proportion of total oligodendrocyte loss ("oligodendrocyte replacement," %; See Methods). Oligodendrocyte replacement after cuprizone cessation followed a sigmoidal pattern, and we quantified it using three-parameter (3P) logistic equations. We were specifically interested in the inflection point (when oligodendrogenesis switches from accelerating to decelerating) and the asymptote of the curve (the plateau of oligodendrocyte replacement, Supplementary Table 2). Oligodendrocyte replacement was delayed relative to loss by approximately four days and plateaued significantly lower than oligodendrocyte loss (Fig. 3h). Mice only replaced on average 60.52±3.03% of lost oligodendrocytes in the seven weeks post-cuprizone; the remyelination response failed to restore baseline oligodendrocyte numbers.

To determine the effects of oligodendrocyte loss and incomplete replacement on neuronal function in forelimb motor cortex, we performed chronic weekly *in vivo* extracellular recordings in both cuprizone-demyelinated and age-matched control mice. *In vivo* multi-site

electrodes record extracellular potentials from neurons within approximately a 150 micron radius of the recording electrode[27]. We confirmed via histology that the proportion of proximally-myelinated neurons in this sampling radius was decreased by over 50% at the cessation of cuprizone administration relative to controls (Extended Data Fig. 5). Neuronal firing rates did not differ between groups prior to or during cuprizone administration, consistent with work in *ex vivo* cortical slices[28]. However, median neuronal firing rates were increased in demyelinated mice versus controls by ~70% in the first week and 40% in the second week post-cuprizone (11.90 vs. 6.92 Hz and 10.68 vs. 7.69 Hz, respectively; Fig. 3i, j), indicating they were hyperexcitable in a manner that temporally correlates with maximum oligodendrocyte loss. By three and four weeks post-cuprizone – when remyelination plateaued – neuronal firing rates in cuprizone-demyelinated mice were indistinguishable from age-matched controls. Taken together, these results demonstrate that cuprizone-mediated demyelination induces aberrant neuronal function in the forelimb region of motor cortex that recovers synchronously with remyelination.

Given that remyelination failed to completely restore baseline oligodendrocyte number but seemed to restore neuronal function, we sought to examine the number, length, and location of sheaths generated by new oligodendrocytes during remyelination. In the first week of remyelination, new oligodendrocytes formed more myelin sheaths than oligodendrocytes generated in the second week of remyelination or in control mice (54.4±3.25 vs. 39.4±1.72 and 42.28±1.30 total sheaths, respectively; Fig. 4a-c; Supplementary Videos 8,9). In healthy mice and during remyelination, sheaths from new oligodendrocytes stabilized to similar lengths within three days after generation (Fig. 4d-f). Therefore, the increased sheath number on new oligodendrocytes in the week following demyelination resulted in a larger total amount of myelin per oligodendrocyte (Fig. 4g). In addition, we found that myelin sheaths of newly generated oligodendrocytes were more often placed in previously unmyelinated areas ("remodeling"; 67.7±3.56% of sheaths) rather than in denuded areas ("remyelinating"; 32.0±3.47% of sheaths), generating a novel pattern of myelination following demyelinating injury (Fig. 4h,i; Supplementary Videos 10,11). These findings indicate that the myelinating capacity of individual oligodendrocytes is increased during early remyelination, and that remyelination by new oligodendrocytes alters the pattern of cortical myelin.

Motor learning modulates oligodendrogenesis after demyelination in a timing-dependent manner

Since we found that motor learning increased both OPC differentiation and oligodendrogenesis in healthy mice (Figs. 1,2), we sought to examine whether it could enhance oligodendrocyte replacement in demyelinated mice. We allotted mice to one of three experimental groups: "no activity," "early-learning" (starting 3 days post-cuprizone), and "delayed-learning" (starting 10 days post-cuprizone; Fig. 5a, b). Behavioral intervention had no effect on the severity of demyelination (Fig. 5c) nor the maximum rate of oligodendrogenesis during remyelination (Fig. 5d).

Mice in the "early-learning" group showed significant performance impairments relative to healthy controls and did not improve their reaching across the learning period, indicating a

failure to acquire the reach task (Fig. 5e; Extended Data Fig. 6). While cuprizone did not alter overall reach attempts, the extent of demyelination was negatively related to performance (Extended Data Fig. 6). Motor deficits were temporally correlated to neuronal hyperexcitability in the forelimb region of motor cortex: firing rate was increased in demyelinated versus healthy mice in the first ten days post-cuprizone, coinciding with the entire early-learning period (Fig. 5f,g). Learning suppressed oligodendrocyte replacement rate by approximately 50% relative to untrained remyelinating mice (1.62±0.13% vs 3.21±0.59%, respectively; Fig 5b,h), resulting in a delayed inflection point of oligodendrocyte replacement (fifteen vs. nine days post-cuprizone, respectively; Fig. 5i). However, the asymptote of oligodendrogenesis did not differ between untrained and early-learning mice. The learning-induced suppression was less severe in remyelinating mice than in healthy controls (50% vs. 75%, respectively; see Fig. 1) and we did not observe an increase in oligodendrogenesis rate post-training (Fig. 5h). Success during learning was unrelated to the asymptote of oligodendrocyte replacement across mice (Extended Data Fig. 6). In sum, motor performance was impaired and motor cortex neurons were hyperexcitable following demyelination, and failing to learn the reach task provided no benefit to oligodendrogenesis during remyelination.

Since mice trained immediately following cuprizone cessation were unable to learn, we trained mice ten days post-cuprizone (ie, the half-maximum of the remyelination response; Fig. 3h). These "delayed-learning" mice showed no overall impairments in reaching performance (Fig. 5j) nor reaching attempts (Extended Data Fig. 6) relative to healthy mice. Again, we found that neuronal hyperexcitability was temporally correlated to reaching success. While demyelinated mice were slightly less successful than healthy controls on the initial day of training (ten days post-cuprizone, when demyelinated mice still show motor cortex neuronal hyperexcitability; Fig. 5k,l), their success rates were indistinguishable from controls by the end of training (seventeen days post-cuprizone). Delayed-learners demonstrated a slight decrease in oligodendrogenesis rate during learning (~30%) that was not statistically different from untrained demyelinated mice (Fig. 5b,m). While the rate of oligodendrogenesis slowed by three weeks post-cuprizone in untrained mice, it did not in delayed-learners. The inflection point of oligodendrocyte replacement was therefore delayed in delayed-learners (thirteen vs. nine days post-cuprizone, respectively; Fig 5n) and oligodendrocyte replacement plateaued substantially higher than in untrained mice (74.56±2.26% vs. 60.52±3.03%, respectively). Success during delayed-learning was not related to oligodendrocyte replacement (Extended Data Fig. 6). In sum, partial remyelination restored both neuronal function and the ability to learn the forelimb reach task, and motor learning following partial remyelination promoted long-term oligodendrogenesis.

To control for motor activity rather than motor learning, mice were trained pre-cuprizone administration and rehearsed the forelimb reach task post-cuprizone (Extended Data Fig. 7). Although demyelinated mice demonstrated performance deficits during rehearsal, rehearsal did not modulate any aspect of remyelination. Only learning the reach task ("delayed-learning"), but not attempting to learn it ("early-learning") nor rehearsing it ("rehearsal"), promoted oligodendrogenesis post-cuprizone.

By seven weeks post-cuprizone, delayed-learning mice replaced over 20% more oligodendrocytes and had over 40% greater density of oligodendrocytes in layers I-III of motor cortex than age-matched, demyelinated, untrained mice (79.24±4.56% vs 58.43±5.26%, and 86.67±5.36 vs. 60.67±4.06, respectively; Fig. 6a-c). Delayed-learning did not modulate the number of sheaths per new oligodendrocyte (Fig. 6d) but did increase the proportion of sheaths that retracted over time (Fig. 6e), similar to observations in healthy mice (Fig. 1i-k). Sheaths from new oligodendrocytes were equally likely to remyelinate denuded axons in both untrained and delayed-learning mice (Fig. 6f). Using mean sheath number per new oligodendrocyte per mouse, we modelled restoration of baseline sheath number and remyelination of denuded axons to a population level. While untrained and delayed-learning mice replaced similar proportions of baseline sheath number prior to behavioral intervention (19.59±0.97% and 24.05±6.54%, respectively; Fig. 6g), delayed-learners replaced almost twice as many lost sheaths as untrained mice post-training (62.22±8.12% versus 34.72±8.84%) due to prolonged oligodendrogenesis (Fig. 5n, Fig. 6a-c). As a result, we project that by seven weeks post-cuprizone, delayed-learners would have replaced almost 90% of their baseline sheath number, versus only 54% in untrained mice (Fig. 6h). Increased sheath generation by delayed-learners resulted in a predicted two-fold increase in remyelination of denuded axons relative to untrained mice (30.19±1.33% versus 16.38±2.37%, respectively; Fig. 6i).

Motor learning promotes the participation of pre-existing mature oligodendrocytes in remyelination

To determine the contribution of pre-existing mature oligodendrocytes to remyelination, we used longitudinal *in vivo* imaging and semi-automated tracing[20] to reconstruct myelin sheaths and connecting processes to the oligodendrocyte cell body (Extended Data Fig. 2). We then tracked myelin sheaths of individual oligodendrocytes throughout cuprizone-mediated demyelination and remyelination (Extended Data Fig. 8; see Methods). Oligodendrocyte survival was variable between mice but did not differ in untrained and delayed-learning groups (12.29±7.32% vs. 20.84±6.60%; Extended Data Fig. 8). After three weeks of cuprizone treatment in untrained mice, all surviving oligodendrocytes experienced sheath loss, and in rare instances (1/19) oligodendrocytes added a new sheath (Fig. 7a-d; Supplementary Videos 12,13). While pre-existing myelin sheaths in healthy mice rarely remodeled (see Fig. 1), cuprizone treatment increased pre-existing sheath retraction in surviving oligodendrocytes (17.0±4.22% vs. 43.8±5.95%; Extended Data Fig. 9). Delayed-learning did not affect the degree of remodeling in pre-existing myelin sheaths during remyelination (Extended Data Fig. 9), but dramatically increased the number of pre-existing oligodendrocytes that generated new myelin sheaths (Fig. 7d,e). Sheath generation in pre-existing oligodendrocytes followed a similar time course to new oligodendrocytes, with sheaths growing during the first three days post-generation before stabilization (Extended Data Fig. 9). In healthy mice, pre-existing oligodendrocytes were never observed generating new sheaths (Extended Data Fig. 9), however, in delayed-learning mice, pre-existing oligodendrocytes were able to generate sheaths even 1.7 months after the onset of imaging, suggesting that the ability to generate myelin sheaths is an extended property of oligodendrocytes (Fig. 7f).

The generation of new sheaths from pre-existing oligodendrocytes was temporally correlated with the onset of forelimb reach training. The number of pre-existing oligodendrocytes generating new sheaths increased by over 40% during learning and persisted in the following weeks (Fig. 7g; Supplementary Video 13,14). As such, delayed-learners had a higher cumulative number of new sheaths generated by surviving oligodendrocytes than untrained mice both during and after learning (Fig. 7h). Myelin sheath loss stagnated in surviving oligodendrocytes after the onset of learning, in contrast to sheath loss in untrained mice which continued for two weeks post-cuprizone (Fig. 7i). The number of lost myelin sheaths was unrelated to sheaths generated on individual oligodendrocytes (Fig. 7j).

As with oligodendrogenesis following learning, sheath addition by pre-existing oligodendrocytes was higher in layer I versus layer II/III of cortex (Fig. 7k,l; Supplementary Video 15). Surviving oligodendrocytes formed new myelin sheaths on both denuded and previously unmyelinated axons (Fig. 7m; Supplementary Videos 16,17). A significantly larger proportion of surviving oligodendrocyte sheaths remyelinated denuded axons relative to newly generated oligodendrocytes (Fig. 7n). The combination of learning-induced cessation of sheath loss and new sheath generation from surviving oligodendrocytes resulted in greater maintenance of the original myelination pattern in delayed learning mice relative to untrained mice (Fig 7o). Pre-existing oligodendrocytes engaging in new myelin sheath deposition showed an increase in overall cell body volume of 141±15% (Extended Data Fig. 10). These findings indicate that, following demyelination, motor learning specifically enhances the ability of pre-existing oligodendrocytes to generate additional myelin and maintain pre-existing sheaths (Supplementary Fig. 1).

Discussion

Tissue regeneration following injury or disease is a long sought-after goal, particularly in the adult nervous system. Oligodendroglia represent one of the few cell types that retain the capacity to regenerate and repair following damage to the adult CNS. Remyelination of denuded axons can restore neuronal function[3], promote neuroprotection[29], and may facilitate functional recovery in CNS diseases characterized by myelin loss[6].

In this study, we show that learning shapes the pattern of myelination in the healthy and remyelinating brain. Longitudinal *in vivo* two-photon imaging of the forelimb motor cortex throughout the learning of a forelimb reach task revealed that learning transiently suppressed oligodendrogenesis but subsequently increased oligodendrocyte generation, OPC differentiation, and retraction of pre-existing myelin sheaths. We found that cuprizone-mediated demyelination induced ~90% oligodendrocyte loss and neuronal firing rate abnormalities in the forelimb region of motor cortex, as well as deficits in motor performance. Motor learning only occurred following partial remyelination and restoration of neuronal function, and resulted in greater oligodendrocyte and myelin sheath replacement. Additionally, motor learning enhanced the ability of surviving oligodendrocytes to participate in remyelination via the generation of new sheaths. These results demonstrate that motor learning can improve remyelination via cortical oligodendrogenesis and myelin sheath formation by surviving oligodendrocytes (Supplementary Fig. 1).

To our knowledge, we are the first to observe a transient learning-induced suppression in oligodendrocyte generation. OPC differentiation was unaffected during this suppression, suggesting that learning may temporarily decrease the survival and integration of differentiated OPCs as mature myelinating oligodendrocytes, in line with previous work in the developing CNS[30]. These nuanced effects may be apparent due to our high intra-individual resolution and regional specificity, whereas previous studies have not parcellated motor cortex based on function[17]. It is possible that location-specific cues suppress the integration of new oligodendrocytes to prevent aberrant myelination during learning, or that metabolic demand imposed by network plasticity during learning[31] may deplete the resources required for the generation and integration of adjacent oligodendrocytes[32]. How these learning-induced changes are communicated to the oligodendrocyte lineage cells remains undefined. Axons form synapses with local OPCs, and neuronal activity can modulate OPC proliferation and differentiation within both the healthy CNS and demyelinated regions[16,33]. This communication may be mediated by the effects of brain-derived neurotrophic factor on both activity-dependent synaptic modulation and oligodendrocyte maturation and myelination[34]. Future work characterizing mechanisms underlying activity-dependent oligodendrogenesis particularly during different life stages will provide additional insight on promoting recovery from demyelinating injury.

We previously reported that environmental enrichment increases oligodendrogenesis but not myelin sheath remodeling in the somatosensory cortex of middle-aged mice[19], yet here we found that motor learning increased both oligodendrogenesis and myelin sheath remodeling in the motor cortex of young adult mice. This disparity may be due to heterogeneity[35], regional variance between somatosensory and motor oligodendrocytes, or age-related decreases in remodeling capacity, as is observed with synaptic plasticity[36]. The role of sheath retraction throughout learning remains to be explored, though recent work suggests this may regulate conduction velocity[37] and allow for increased axonal branching. Concurrent multi-color *in vivo* imaging of reach-related neurons and myelin sheaths throughout learning will clarify how neurons and oligodendrocytes interact during circuit consolidation.

The consequences of demyelination on the function of intact cortical neural circuits is not well understood. We found that neural firing rate increased following demyelination, and resulted in hyperexcitability of forelimb motor cortex. Despite effects of copper chelation on NMDAR and AMPAR currents and neuronal excitability[38], we found no effect of cuprizone treatment on concurrent neuronal firing rate *in vivo*, similar to previous accounts of *ex vivo* whole cell recordings[28]. Hyperexcitability is a common feature of neurodegenerative diseases and can be a consequence of increased cellular stressors, including elevated intracellular calcium load[39] as is observed in experimental autoimmune encephalomyelitis (EAE) models of MS[40]. The accumulation of cellular stress as a result of demyelination may be a potential cause of neurodegeneration seen in patients with progressive MS. In addition to cell-autonomous mechanisms, hyperexcitability may also result from changes in the complex excitatory and inhibitory balance within motor cortex control of movement, for example via alterations in the myelination of thalamocortical input, corticospinal output axons, or local circuitry. In neurodegenerative disorders, local circuit processing alterations produce hyperexcitability[41], which predicts motor impairments in both human patients and

animal models[42,43]. We found that neuronal activity in remyelinating mice was indistinguishable from healthy controls when superficial motor cortex remyelination plateaued, and that this partial remyelination rescued motor deficits. These data show a clear link between cortical myelin content, neuronal function, and motor behavior. Future work characterizing the cell-type specific changes in neuronal excitability[44] and plasticity[45], along with circuit-level alterations in excitatory and inhibitory balance within motor cortex[46] will provide insights into the cellular and circuit origins of demyelination-induced hyperexcitability.

Recent analysis of tissue from MS patients suggests that shadow plaques are incompletely demyelinated lesions or lesions remyelinated by pre-existing oligodendrocytes[7,8]. Our data clearly demonstrate both scenarios occur following demyelination. Furthermore, we show that the remyelinating potential of pre-existing mature oligodendrocytes is modulated by learning. While the majority of surviving oligodendrocytes contributed new myelin sheaths following learning, the variability in magnitude of this response raises questions about what drives certain oligodendrocytes to generate more myelin than others. Proximity to a learning-relevant neural circuit may modulate the amount of new myelin deposited by surviving oligodendrocytes[47,48]. Exploring whether surviving oligodendrocytes preferentially myelinate axons that they are already ensheathing may provide insight as to whether direct axo-myelinic communication[69] plays a role in initiating the remyelination response in pre-existing oligodendrocytes. Continued reduction in cell soma size and progressive compaction of chromatin are hallmarks of OPC maturation into myelinating oligodendrocytes[49,50]. Cell soma volume increases during surviving oligodendrocyte remyelination suggest that epigenetic regulation of gene expression may regulate the generation of new myelin, similar to recent findings in MS patient tissue[7]. Identification of gene expression changes in mature oligodendrocytes engaging in new sheath deposition could provide insight into the molecular mechanisms driving remyelination by mature oligodendrocytes and provide new therapeutic targets to promote remyelination.

Behavioral interventions used to support motor function in MS patients[14] may also engage endogenous mechanisms to stimulate myelin addition after injury. Notably, motor learning implemented after the onset of remyelination prolonged the duration of oligodendrogenesis, increased oligodendrocyte replacement, nearly restored baseline sheath number, and promoted the remyelination of denuded axons by both new and surviving oligodendrocytes. Overall, our findings argue that specifically timed therapeutic interventions designed to promote oligodendrogenesis and engage mature oligodendrocytes in myelin repair may enhance remyelination and speed functional recovery in demyelinating disorders.

Methods

Animals

All animal experiments were conducted in accordance with protocols approved by the Animal Care and Use Committee at the University of Colorado Anschutz Medical Campus. Male and female mice used in these experiments were kept on 14h light/10h dark schedule with ad libitum access to food and water, aside from training-related food restriction (see Forelimb Reach Training). All mice were randomly assigned to conditions and were

precisely age-matched (±5 days) across experimental groups. *NG2-mEGFP* (Jackson stock #022735) and congenic C57BL/6N *MOBP-EGFP* (MGI:4847238) lines, which have been previously described[19,23], were used for two-photon imaging. Wild-type C57\B6N Charles River wild-type mice were used in electrophysiological experiments.

Two-photon microscopy

Cranial windows were prepared as previously described[19]. Six- to eight-week-old mice were anesthetized with isoflurane inhalation (induction, 5%; maintenance, 1.5–2.0%, mixed with 0.5 L/min O2) and kept at 37 °C body temperature with a thermostat-controlled heating plate. After removal of the skin over the right cerebral hemisphere, the skull was cleaned and a 2×2 mm region of skull centered over the forelimb region of primary motor cortex (0 to 2 mm anterior to bregma and 0.5 to 2.5 mm lateral) was removed using a high-speed dental drill. A piece of cover glass (VWR, No. 1) was then placed in the craniotomy and sealed with Vetbond (3M) and subsequently dental cement (C&B Metabond). A 5mg/kg dose of Carprofen was administered subcutaneously prior to awakening and for three additional days for analgesia. For head stabilization, a custom metal plate with a central hole was attached to the skull. *In vivo* imaging sessions began 2–3 weeks post-surgery and took place 2–3 times per week (see imaging timelines in Figs. 1–3,5). During imaging sessions, mice were anesthetized with isoflurane and immobilized by attaching the head plate to a custom stage. For *MOBP-EGFP* experiments, images were collected using a Zeiss LSM 7MP microscope equipped with a BiG GaAsP detector using a mode-locked Ti:sapphire laser (Coherent Ultra) tuned to 920 nm. *NG2-mEGFP* mice were imaged using a Bruker Ultima Investigator microscope equipped with Hamamatsu GaAsP detectors and a mode-locked Ti:sapphire laser (Coherent Ultra) tuned to 920 nm. The average power at the sample during imaging was 5–30 mW. Vascular and cellular landmarks were used to identify the same cortical area over longitudinal imaging sessions. *MOBP-EGFP* image stacks were acquired with a Zeiss W "Plan-Apochromat" 20X/1.0 NA water immersion objective giving a volume of 425 μm × 425 μm × 336 μm (1,024 × 1,024 pixels; corresponding to layers I–III, 0–336 μm from the meninges) from the cortical surface. *NG2-EGFP* image stacks were acquired with a Nikon LWD Plan Fluorite 16X/0.8 NA water objective with a volume of 805 μm × 805 μm × 336 μm (2,048 × 2,048 pixels; corresponding to layers I–III, 0–336 μm from the meninges).

SCoRe microscopy

Spectral confocal reflectance microscopy (SCoRe) was performed as previously described[51]. For the *MOBP-EGFP* SCoRE/two-photon validation experiments, *in vivo* image stacks were acquired on an Olympus F1000MPE upright multiphoton microscope (DIVER). Single-photon confocal microscopy was performed using 488, 543, and 633nm laser lines combined with appropriate emission filters and descanned Olympus detectors. Two-photon microscopy of *MOBP-EGFP* fluorescence was performed immediately following SCoRe imaging using a mode-locked Insight X3 laser (Spectra-Physics) tuned to 920nm and non-descanned Olympus detectors. All images were obtained using an Olympus 20X/1.0 NA water immersion objective (XLUMPLFLN20XW). SCoRe image channels were summed, registered to the two-photon data, and then analyzed for SCoRe/two-photon colocalization using FIJI/ImageJ.

Cuprizone-mediated demyelination

Cortical demyelination was induced in our congenic C57\B6N *MOBP-EGFP* mice using 0.2% Cuprizone (Sigma Chemical #C9012), stored in a glass desiccator at 4°C. Cuprizone was mixed into powdered chow (Harlan) and provided to mice in custom feeders (designed to minimize exposure to moisture) for three weeks on an ad libitum basis. Feeders were refilled every 2–3 days, and fresh cuprizone chow was prepared weekly. Cages were changed weekly to avoid build-up of cuprizone chow in bedding, and to minimize reuptake of cuprizone chow following cessation of diet via coprophagia. We used a 3-week partial cortical demyelination model (resulting in 88.3±2.9% oligodendrocyte loss in motor cortex) to allow us to track the same area of interest over time using surviving oligodendrocytes, and to investigate the behavior of surviving oligodendrocytes. Given that cuprizone was ingested on a voluntary basis, we controlled for variation in dosage in several ways. First, we weighed a subset of mice (n = 19) before and after cuprizone diet to ensure no weight loss had occurred. We found that on average, mice gained weight during cuprizone administration, confirming their consumption of the drug (Paired student's t-test, t(18) = 2.32, p = 0.03). Second, we investigated variation in total oligodendrocyte loss. There was variation in maximum oligodendrocyte loss (50–100%), and oligodendrocyte loss and gain had a partially homeostatic relationship in that the amount of loss significantly predicted the subsequent amount of oligodendrocyte gain (Fig. 3g; Extended Data Fig. 5). To control for variation in total oligodendrocyte loss, and its subsequent effects on oligodendrocyte gain, we therefore measured oligodendrocyte gain relative to the severity of loss using the following equation:

$$oligodendrocyte\ replacement\ (\%) = \frac{New\ oligodendrocytes}{Maximum\ oligodendrocyte\ loss} \times 100$$

Forelimb reach training

Mice were weighed, habituated to a training box for 20 minutes, and deprived of food 24 hours prior to training. The training box was fitted with a window providing access to a pellet located on a shelf 1cm anterior and 1mm lateral to the right-hand side of the window. After one session of initial habituation, training sessions began daily for 20 minutes. Mice learned to reach for the pellet using their left hand. Successes were counted when the mouse successfully grabbed the pellet and transported it inside the box. Errors were qualified in three ways: "Reach error" (the mouse extends its paw out the window but does not grab the pellet), "Grasp error" (the mouse reaches the pellet but does not successfully grasp onto it), and "Retrieval error" (the mouse grasps the pellet but does not succeed in returning it to the box; Supplementary Video 1). Mice were kept on a restricted diet throughout training to maintain food motivation but were weighed daily to ensure weight loss did not exceed 10%. For forelimb reach training, mice underwent habituation (average of ~2 days of exposure) followed by training until seven consecutive days of training with reach attempts were recorded. For the rehearsal of the forelimb reach task, mice performed the reach task in a 20-minute session, 5 days per week over three weeks. Similar to previously published findings, over 90% of mice trained in forelimb reach context were able to learn the task[18]; mice were excluded if they were not able on a single day to succeed in at least 10% of reaches (Extended Data Fig. 1). To control for any batch or experimenter effects in forelimb reach

training results, behavioral performance was only compared for mice trained by the same experimenter within the same batch (i.e., control and experimental mice were only compared if trained at the same time by the same experimenter).

Immunohistochemistry

Mice were anesthetized with an intraperitoneal injection of sodium pentobarbital (100 mg/kg b.w.) and transcardially perfused with 4% paraformaldehyde in 0.1 M phosphate buffer (pH 7.0–7.4). Brains were postfixed in 4% PFA for 1 h at 4 °C, transferred to 30% sucrose solution in PBS (pH 7.4), and stored at 4 °C for at least 24 h. Brains were extracted, frozen in TissuePlus O.C.T, and sectioned coronally or axially (bregma 0 to 2 mm) at 50 μm thick. Immunostaining was performed on free-floating sections. Sections were pre-incubated in blocking solution (5% normal donkey serum, 2% bovine g-globulin, 0.3% Triton X-100 in PBS, pH 7.4) for 1–4 h at room temperature, then incubated overnight at 4 °C in primary antibody (listed along with secondary antibodies in Supplementary Table 1). Secondary antibody incubation was performed at room temperature for 2 h. Sections were mounted on slides with Vectashield antifade reagent (Vector Laboratories). Images were acquired with a laser-scanning confocal microscope (Zeiss LSM 510).

Image Processing and Analysis

Image stacks and time-series were analyzed using FIJI/ImageJ. All analysis was performed on unprocessed images except in surviving oligodendrocyte myelin sheath analysis images, which were pre-processed by with a Gaussian blur filter (radius = 1 pixels) to denoise. When generating figures, image brightness and contrast levels were adjusted for clarity. For the pseudocolor display of individual myelin sheaths or OPCs (Figs. 1–4,6,7; Extended Data Figs. 2,4,8–10; Supplementary Videos 2,3,5,6,8–17), a max projection of the region of interest was generated and was manually segmented and colorized. Longitudinal image stacks were registered using FIJI plugins 'Correct 3D drift'[52] or 'PoorMan3DReg'. When possible, blinding to experimental condition was used in analyzing image stacks from two-photon imaging. To ensure the validity of oligodendrocyte lineage cell tracking, we performed interrater reliability on a subset of images and found a highly significant correlation between raters ($R^2 = 0.998$, $p < 0.0001$).

Cell Tracking—Custom FIJI scripts were written to follow oligodendrocytes in four dimensions by defining EGFP+ cell bodies at each timepoint, recording xyz coordinates, and defining cellular behavior (new, dying, proliferating, differentiating, or stable cells). Mature oligodendrocyte and OPC migration, proliferation, death, and differentiation were defined as previously described[19,23]. Differentiation events were recorded as the time point immediately preceding the total loss of *NG2-mEGFP* fluorescence. OPC and oligodendrocyte gain and loss were quantified cumulatively relative to baseline cell number to account for variation in starting cell number. Rate of oligodendrocyte gain was quantified as the percent change in gain over the amount of time elapsed.

Identification of surviving oligodendrocytes—A subset of surviving oligodendrocytes exhibited drastic changes in morphology during remyelination in the form of cell body expansion, sheath addition, and increase in EGFP expression (Extended Data

Fig. 8–10). To ensure that these oligodendrocytes were in fact individual surviving oligodendrocytes and not new oligodendrocytes generated in a similar location that myelinated similar axonal locations, we employed several criteria for inclusion in our final dataset. Due to the stringency and conservative nature of these criteria, we consider our findings to likely be an underestimate of the capacity of surviving oligodendrocytes to generate new myelin sheaths:

1. Change in cell soma centroid (< 2.5 standard deviations from the mean)

2. Percentage of sheath retention (> 10% of original sheaths)

3. Change cell soma volume (< 700 μm^3)

4. Protracted sheath addition (> 6 days)

5. Semi-automated tracing of new sheath to OL surviving cell body (using Simple Neurite Tracer)

6. Distance between surviving and new oligodendrocyte cell bodies at time point of sheath generation (> 50 μm)

We measured the change in centroid position of surviving oligodendrocyte cell bodies from baseline to day of peak remodeling—i.e. the day where the largest number of sheaths were added by a given oligodendrocyte. We ensured that the 3D location of individual surviving oligodendrocytes did not change by more than 2.5 standard deviations from the mean displacement of reference objects measured within the same stack (5.459±2.373 μm; Extended Data Fig. 8). Since myelin sheath loss occurs significantly earlier than cell body loss in oligodendrocyte cell death (Fig. 3d,e) and a new oligodendrocyte could be generated in the same location immediately following the death of the original oligodendrocyte, we only included surviving oligodendrocytes that conserved at least 10% of their original processes (mean percent conserved processes = 75.6±4.45%). There is an increase in the frequency of pairs and rows of oligodendrocytes with adjacent cell somas in the aging brain[53]. Since the axial resolution of our two-photon microscope is ~2.6 μm, we should be able to resolve two directly adjacent oligodendrocytes in the z-direction. To ensure that this is the case, we took several additional steps to rule out the addition of a new oligodendrocyte generated immediately adjacent in the z-axis. Reduction of cell soma size is a hallmark of the maturation of OPCs into myelinating oligodendrocytes[49,50]; therefore, we measured the cell soma volume of newly generated oligodendrocytes (Extended Data Fig. 8). Next, we measured each surviving oligodendrocyte at baseline and at the day of peak remodeling to determine the change in cell soma volume. Assuming a z-distance of 0 μm between two cells, we excluded oligodendrocytes that grew more than 700 μm^3, the volume of the smallest new oligodendrocyte measured (Extended Data Fig. 8). Additionally, we ensured that this growth was not unidirectional (as you would see with the addition of an adjacent oligodendrocyte cell body), but rather that the oligodendrocyte cell body expanded in multiple directions around the centroid position. Previous studies have indicated that new oligodendrocytes have a limited period in which to generate all of their myelin sheaths, a few hours in the developing zebrafish[54] and less than 18 hours in vitro[55]. We found that new oligodendrocytes generate all sheaths within 0–3 days of generation in mice (n_{mice} = 11; n_{cells} = 26, Fig. 4). If a new oligodendrocyte was generated directly adjacent to a surviving

oligodendrocyte, we would predict that all additional myelin sheaths would be added within this time frame. Therefore, we required that surviving oligodendrocytes that added more than 4 sheaths— approximately 10% of the average sheaths generated by an oligodendrocyte — must have added these new sheaths over multiple, non-consecutive imaging time points (Extended Data Fig. 8, Supplementary Video 14). Using these criteria, two oligodendrocytes were excluded from the final dataset as they may have represented the addition of a new oligodendrocyte in a similar location. One oligodendrocyte violated both the change in centroid requirement and protracted sheath addition requirement (change in centroid = 19.3266 μm, and 8 sheaths were added at one time point) and the other violated the terms for protracted sheath addition (over 10 sheaths added within two consecutive timepoints). Three other surviving oligodendrocytes were excluded from new sheath analysis because new oligodendrocytes were generated within 50 μm of the surviving oligodendrocyte cell body on the day of surviving oligodendrocyte sheath addition. The surviving oligodendrocyte dataset was analyzed by multiple, blinded raters and, where blinding was not possible (e.g. due to recognizable landmarks in the image stacks), all counts were validated by multiple raters. As an additional measure, only new sheaths with processes that could be traced back to the surviving oligodendrocyte cell body with Simple Neurite Tracer were included in our final dataset (Extended Data Fig. 2; Supplementary Video 3). Finally, myelin debris prevented faithful analysis of processes and sheaths from oligodendrocytes in the timepoint following cuprizone treatment and therefore we excluded the time point immediately after the removal of cuprizone (i.e. 0d) from analysis.

Myelin sheath analysis of individual oligodendrocytes—*In vivo* z-stacks were collected from *MOBP-EGFP* mice using two-photon microscopy. Z-stacks were processed with a 1-pixel Gaussian blur filter to aid in the identification of myelin internodes. Myelin paranodes and nodes of Ranvier were identified as described previously[73], by increase in fluorescence intensity for paranodes and a decrease to zero in EGFP fluorescence intensity for nodes. Myelin sheaths from surviving oligodendrocytes were traced using Simple Neurite Tracer at day −25 and day 21. In normal learning mice, two additional time points were traced that corresponded to day 0 and day 9 of training. To account for differences in measurement due to tracing, a subset of sheaths were traced five times at a single time point. Traces of the same sheath differed by less than 5.56 μm. Therefore, sheaths were defined as stable if their baseline and final lengths changed less than 5.56 μm. Sheaths that grew more than 5.56 μm were considered growing and those that shrank more than 5.56 μm were considered retracting.

For myelin sheath analysis of surviving oligodendrocytes, surviving oligodendrocytes that resided within a volume of $425 \times 425 \times 100 \ \mu m^3$ from the pial surface were considered in Layer I and cells $100–336 \ \mu m^2$ were considered Layer II/III. Myelin sheaths of surviving oligodendrocytes were tracked throughout time with the same FIJI scripts used for cell tracking. Only sheaths with visible processes back to the surviving cell body in at least one time point were counted. Sheaths were defined as new, lost, or persisting. Persisting sheaths lasted for the entire imaging time course; new sheaths appeared after day 0; and lost sheaths disappeared before the end of the imaging time course and were not visible for at least 2 consecutive timepoints. Our average total sheath count per surviving oligodendrocyte was

30.2±1.32. Assuming a normal range of 45±4 sheaths/oligodendrocyte[73], our average sampling was 67–74% of all sheaths.

Electrophysiology

Chronic *in vivo* recordings were conducted during 20 minute forelimb reach training sessions before, during, and after cuprizone treatment. A single 1.6mm vertical NeuroNexus recording electrode was chronically inserted into primary motor cortex (300μm anterior to bregma, 1.5mm lateral bregma) contralateral to the trained forelimb. Data was recorded using Cheetah acquisition software at 30kHz (NeuroNexus), and single unit activity was clustered using Spike Sort 3D (Neuralynx). Isolation Distance and L-Ratio was used to quantify cluster quality and noise contamination[81]. Spike data was binned at 10ms and trial-averaged. Heatmaps report average firing rate during 500 ms time window when the animal was not engaged in reach behavior.

Statistics

A detailed and complete report of all statistics used, including definitions of individual measures, summary values, sample sizes, and all test results can be found in Supplementary Table 2. Sample sizes were not predetermined using statistical methods, but are comparable to relevant publications[19,23]. All data were initially screened for outliers using IQR methods. In Fig. 7j, a single outlier oligodendrocyte was removed after testing because it drove significance in the correlation (see Supplementary Table 2 for details). Homozygous, C57BL/6N congenic *MOBP-EGFP* mice were bred with C57BL/6N mice to generate litters of experimental mice that were hemizygous for the *MOBP-EGFP* transgene. All mice in a litter underwent cranial window surgery, concurrent two-photon imaging timelines, and were designated to be a "batch". When possible, experimental groups were replicated in multiple batches with multiple experimental groups per batch. However, due to the longitudinal nature of our study, and the clarity of cranial windows used to conduct two-photon imaging, we could not predict which mice would produce full datasets when assigning them to experimental conditions. As a result, not all batches contain all experimental groups, and we controlled for batch statistically. Statistical analyses were conducted using JMP (SAS) or MATLAB (MathWorks). We first assessed normality in all datasets using the Shapiro-Wilk test. When normality was violated, we used non-parametric tests. When normality was satisfied, we used parametric statistics including paired or unpaired two-tailed Student's t-tests (depending on within- or between-subjects nature of analysis), or ANOVA with Tukey's HSD post-hoc tests. Two-tailed tests and α 0.05 were always employed unless otherwise specified. For statistical mixed modelling, we used a restricted maximum likelihood (REML) approach with unbounded variance component, and least-squared Tukey's HSD post-hoc tests. All models were conducted with either one or two fixed effects, in which case we ran full factorial models. For all models, we used "Mouse ID" as a random variable, and this random variable was nested within "batch" if data came from separate batches. Where we found significant effects, we subsequently calculated effect size using test-appropriate approaches. For data visualization, all error bars represent standard error on the mean, all bar graphs denote means, and all box plots illustrate median and interquartile range (IQR) unless otherwise specified. We used three-parameter (3P) logistic equation

modelling to fit sigmoidal curves bound between an asymptote of 0 (baseline) and an estimated plateau to oligodendrocyte accumulation (either loss or gain) across time.
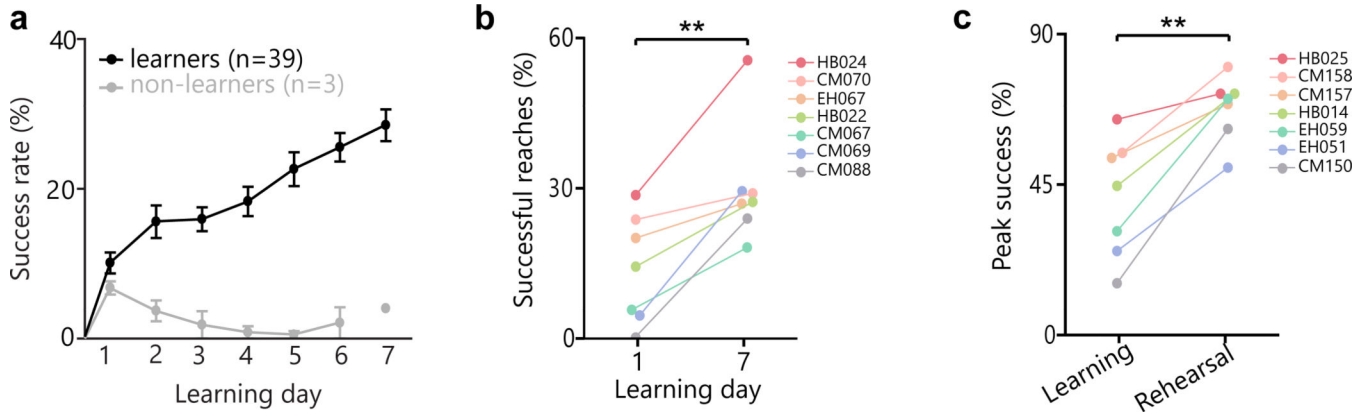
Extended Data

Extended Data Fig. 1: Learning and rehearsal of a forelimb reach task induce skill refinement.
a, A large majority (93%) of mice successfully learn to perform the forelimb reach task. "Learners" (black) gradually improve their reaching performance over the seven days of training, whereas "non-learners" (grey) show a progressive decrease in success rate and eventually stop making reach attempts around day 4. Note, the lone point in the "non-learner" group at day 7 is due to only one mouse making attempts on the last day of training. The other two mice had stopped trying. b, Successful reaches (%) significantly increase between learning days 1 and 7 (paired samples t-test; t(6) = 4.80, p = 0.003) for mice placed in "learning" group. c, Peak performance during rehearsal (successful reaches; %) is significantly higher than peak performance during learning (paired samples t-test; t(6) = 5.47, p = 0.0016) for mice placed in "rehearsal" group. Individual colors and traces reflect performance by individual mice. *p < 0.05, **p < 0.01, ***p < 0.001. Bars and errors represent Mean±SEM, for statistics see Supplementary Table 2.1.
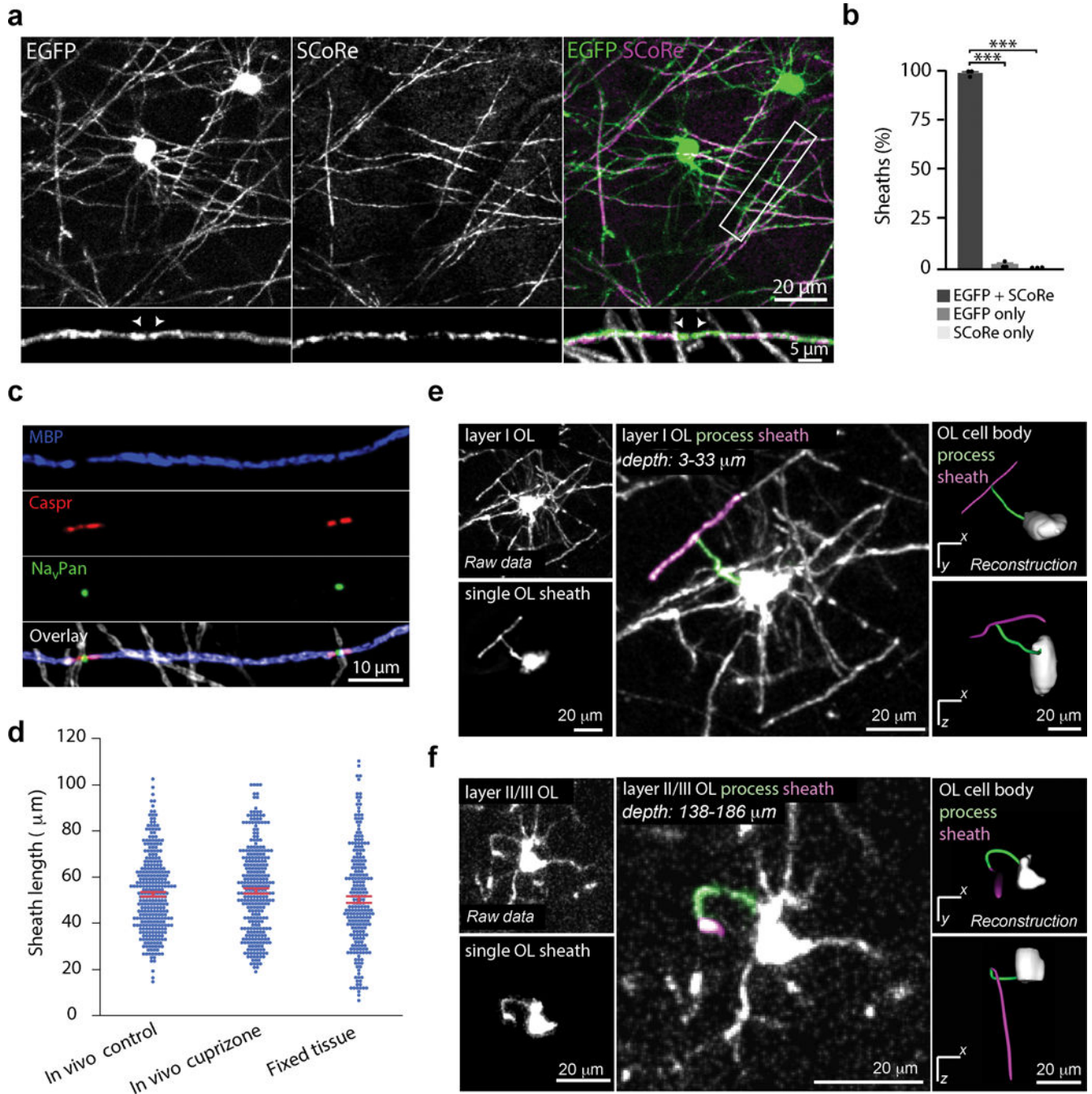
Extended Data Fig. 2: *In vivo* **imaging of** *MOBP-EGFP* **faithfully reflects myelin sheath presence, length, and connection to oligodendrocyte cell body.**

a, b, Maximum projections of cortical oligodendrocytes showing 98.24±0.92% colocalization of *in vivo MOBP-EGFP* and SCoRe signal in myelin sheaths, confirming *MOBP-EGFP* faithfully reflects presence of myelin (ANOVA, n_{mice} = 3, $F_{2,6}$ = 5596.220, p < 0.0001). **c**, Maximum projection of 4% paraformaldehyde fixed tissue, stained for myelin (blue, MBP), paranodes (Caspr, red), and sodium channels (NavPan, green). **d**, No significant difference between sheath lengths measured using Simple Neurite Tracer in *in*

vivo two-photon images of control and cuprizone-treated *MOBP-EGFP* mice, and in confocal images of sheaths immunostained for MBP in fixed tissue ($n_{sheaths}$ = 306, 297 and 233, respectively; points represent individual sheaths; ANOVA; $F_{2,833}$ = 2.53, p > 0.08; red points and error bars represent group means±SEM). **e,f** Semi-automated tracing with Simple Neurite Tracer faithfully reconstructs oligodendrocyte myelin sheaths and their connecting processes to the cell soma in layer I (e) and layer II/II (f). Top left: Maximum projection of an oligodendrocyte (OL) imaged using *in vivo* two-photon microscopy, spanning a depth of 3–33 μm (e) and 138–186 μm (f) in motor cortex. Bottom left: maximum projection of an isolated single sheath and process attached to the oligodendrocyte cell body. Center: maximum projection and pseudo-colored sheath and process (sheath and process pseudo-colored). Right: Three-dimensional (3D) reconstruction of the same oligodendrocyte generated from the raw *in vivo* imaging data using the Simple Neurite Tracer plugin in FIJI. View of 3D volume in xy plane from below (top) and view of 3D volume through z (bottom). *p < 0.05, **p < 0.01, ***p < 0.001. Bars and errors represent Mean±SEM, for statistics see* Supplementary Table 2.1.
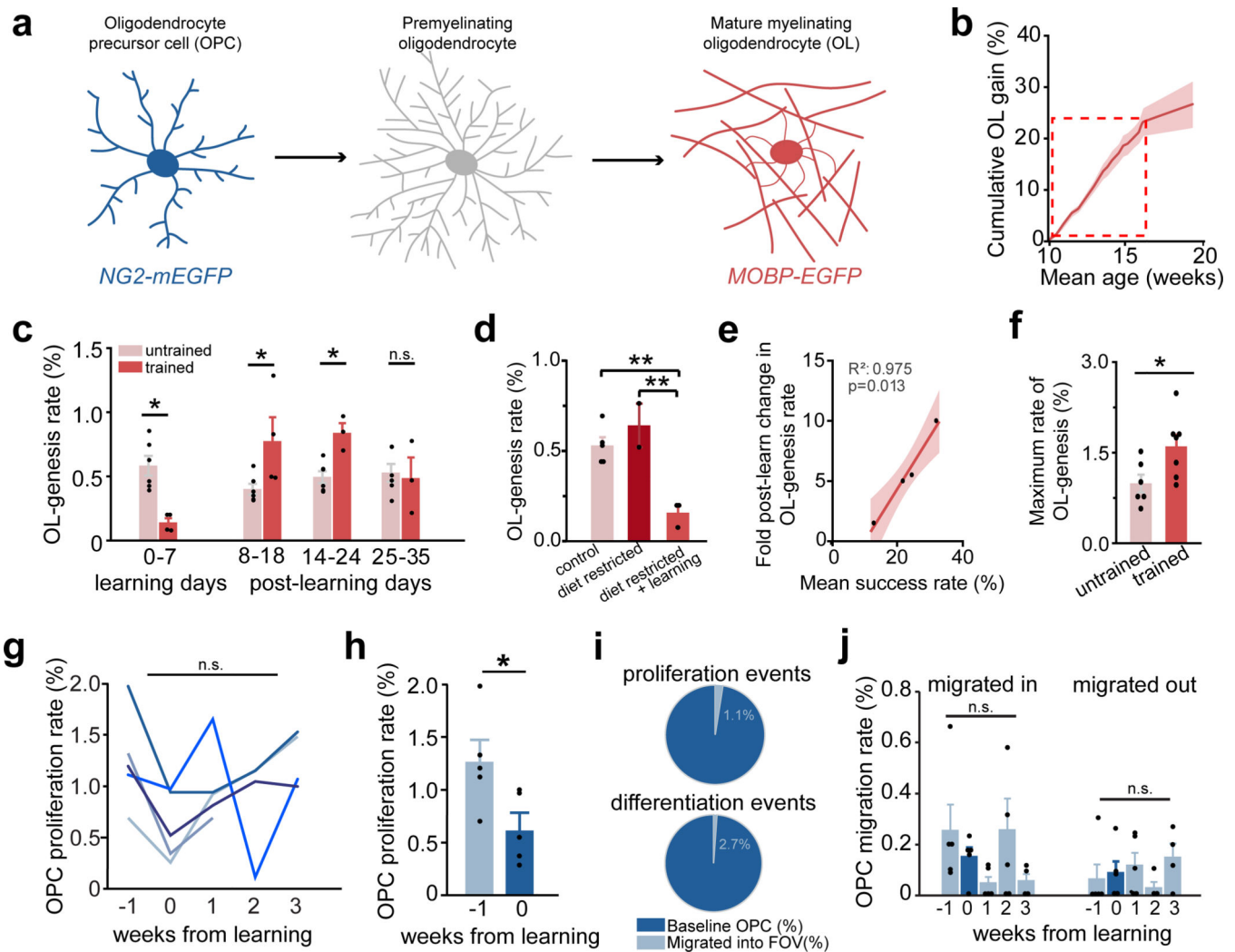
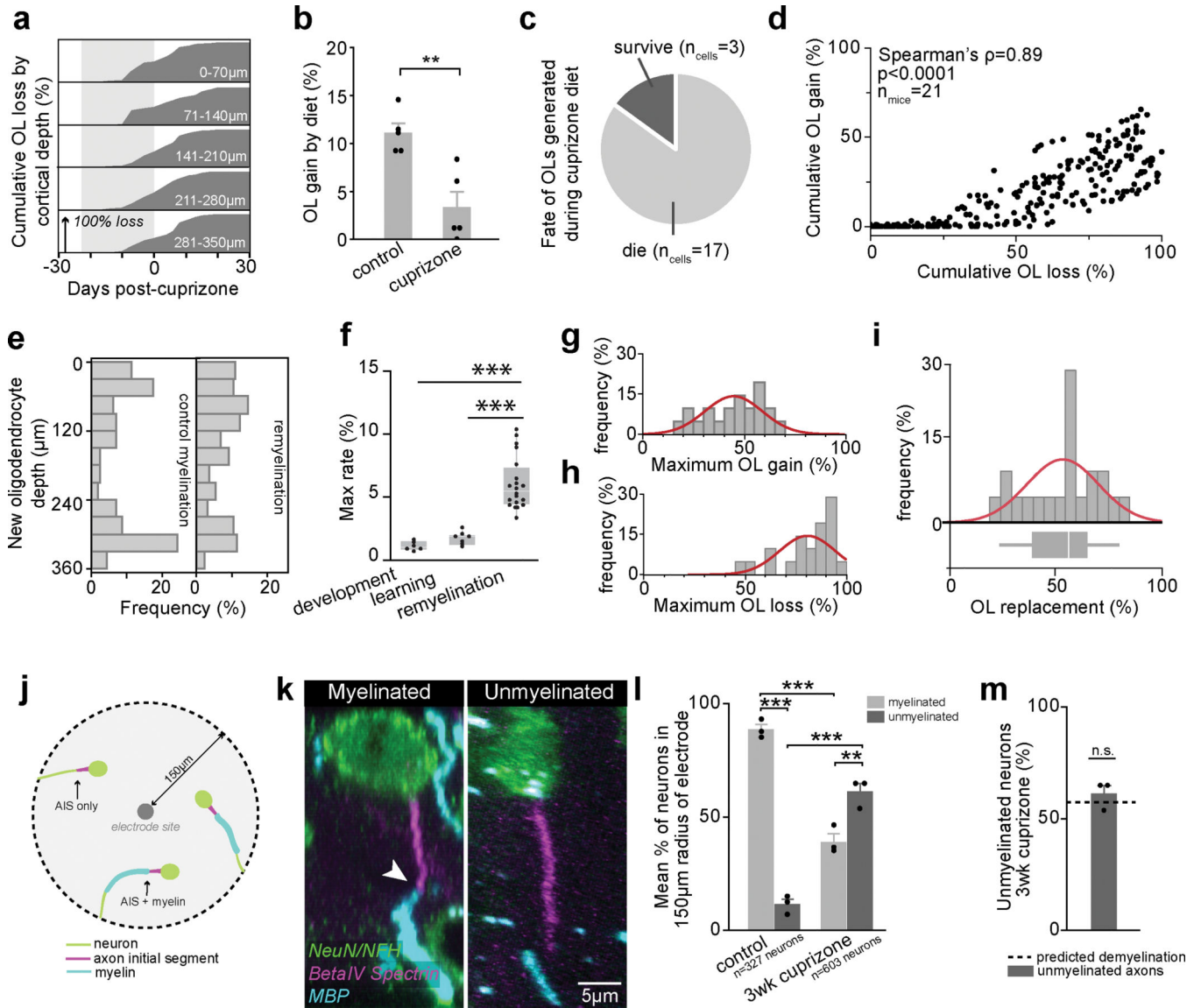**Extended Data Fig. 3: Oligodendrocyte lineage cell dynamics throughout motor learning.**
a, Genetic lines for *in vivo* imaging of oligodendrocyte precursor cells (OPCs; *NG2-mEGFP*) and oligodendrocytes (OLs; *MOBP-EGFP*). **b,** Motor cortex oligodendrogenesis from age 10–20 weeks across six mice, showing a plateau ~17 weeks. Dashed box represents age during standard experimental timeline. **c,** Rate of oligodendrogenesis is altered in learning vs. untrained mice during learning (Wilcoxon Rank-Sum, p = 0.014), days 8–18 post-learning (p = 0.038), and days 14–24 post-learning (p = 0.024). No differences are observed by days 25–35 post-learning (p > 0.9). Points represent mice. **d,** Main effect of diet restriction on oligodendrogenesis rate (%; ANOVA; $F_{2,8}$ = 18.13, p = 0.001). Diet-restricted and non-diet-restricted controls have higher rates of oligodendrogenesis than diet-restricted learning mice (Tukey's HSD, p = 0.001 and p = 0.005, respectively). **e,** Mean success rate is related to fold change in oligodendrogenesis rate post-learning (R-square = 0.98, p = 0.01). Line and shaded area represent fit and 95% confidence of fit. **f,** Trained mice (learning and rehearsal) have increased maximum rates of oligodendrogenesis relative to controls (t(10.61) = –2.49, p = 0.03). **g, h,** Proliferation rates from Fig. 2d; colors represent individual mice. All mice show reduced proliferation rate

during learning relative to baseline ($t(4) = -3.89$, $p = 0.018$; paired student's t-test), but no main effect of time on proliferation rate across the five weeks of experiment - possibly due to high variability post-learning ($F_{4,15} = 2.341$). **i**, Only a minority of proliferation and differentiation events occurred in OPCs that had migrated into the field of view throughout the course of the experiment. **j**, No effect of learning on rate of migration into or out of the field of view. *$p < 0.05$, **$p < 0.01$, ***$p < 0.001$. Bars and errors represent Mean±SEM, for statistics see* Supplementary Table 2.1.
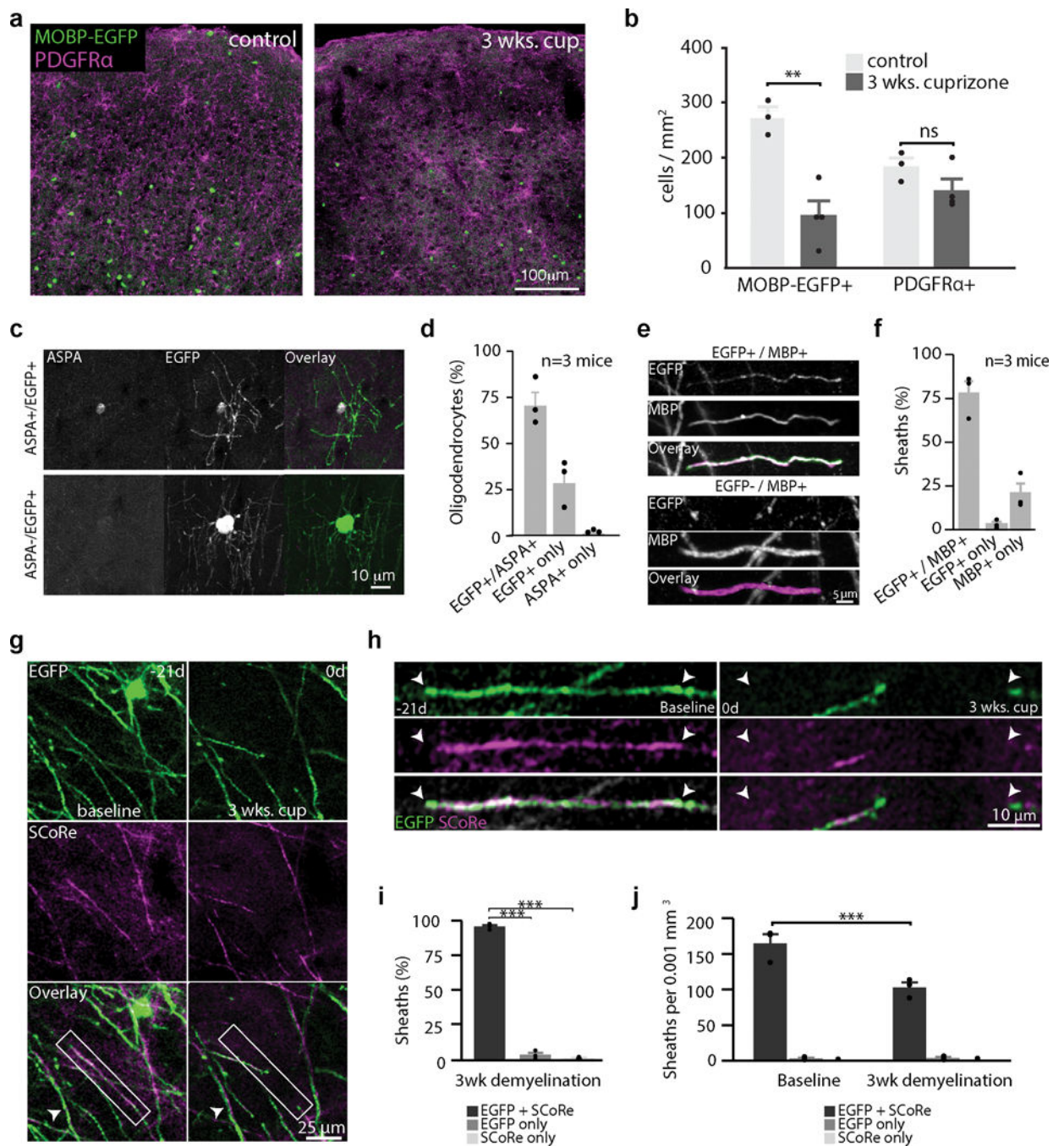
Extended Data Fig. 4: Cuprizone treatment results in loss of myelin and oligodendrocytes.
a, b, Mean density of EGFP+ and PDGFRα+ cells in control and cuprizone-treated *MOBP-EGFP* mice; individual points represent individual mice. Interaction effect between drug (control vs. cuprizone) and cell type (EGFP+ vs PDGFRα+; ($F_{1,5}$=22.39, p=0.0052) to predict cell density. While EGFP+ cell density is decreased in cuprizone-treated mice relative to controls (Tukey's HSD; p=0.0086), there is no difference in PDGFRα+ cells between groups (p>0.5). **c,** Maximum projection of a EGFP+/ASPA+ oligodendrocyte (top) and a EGFP+/ASPA- oligodendrocyte (bottom). Note the large size of the ASPA-/EGFP+ cell

soma suggesting it is a recently born oligodendrocyte in the early stages of the maturation process. **d**, After three weeks of cuprizone treatment, $70.73\pm12.78\%$ of oligodendrocytes are EGFP$^+$/ASPA$^+$, $0.97\pm0.84\%$ of cells are ASPA$^+$/EGFP$^-$, while the remainder are EGFP$^+$-only (n_{mice}=3, n_{cells}=185). **e**, Maximum projection of an MBP$^+$ myelin sheath with (top) and without EGFP (bottom) after three weeks of cuprizone. **f**, After three weeks of cuprizone, $76.21\pm7.11\%$ of sheaths are MBP$^+$/EGFP$^+$, and $20.6\pm5.79\%$ of sheaths are MBP$^+$/EGFP$^-$ (n_{mice}=3, $n_{sheaths}$=351). **g,h** Maximum projections of oligodendrocytes showing colocalization of *in vivo MOBP-EGFP* and SCoRe imaging for myelin both before cuprizone administration (–21 days) and immediately following its removal (0 days). Note the surviving sheath (white arrow). **i**, Following 3 weeks of cuprizone diet, most myelin sheaths are MOBP-EGFP$^+$/SCoRe$^+$ (95.71 ± 1.16; ANOVA, $F_{2,6}$=2012.94, p<0.0001). **j**, Cuprizone administration modulates sheath density ($F_{2,10}$=14.43, p=0.001). Cuprizone-fed mice have a reduced density of MOBP-EGFP$^+$/SCoRe$^+$ positive sheaths relative to controls (p=0.0001), but no difference in GFP-only or SCoRe-only sheaths. *p<0.05, **p<0.01, ***p<0.001. Bars and errors represent Mean±SEM, for statistics see* Supplementary Table 2.3.

Extended Data Fig. 5: Dynamics of oligodendrocyte generation and loss during cuprizone treatment.

a, Oligodendrocyte loss occurred evenly across cortical depths. Shaded area represents cuprizone diet. **b**, Oligodendrogenesis is suppressed during cuprizone diet (n = 5 mice per group; t(6.54) = 4.10, p = 0.005; Student's t-test). **c**, 85% of oligodendrocytes generated during cuprizone diet die within three weeks. **d**, Oligodendrocyte loss predicts gain (Spearman's ρ = 0.89). **e**, Oligodendrocytes generated during remyelination are distributed across cortex similarly to developmental oligodendrogenesis (Wilcoxon Rank-sum, p > 0.1). **f**, Remyelination alters oligodendrogenesis rates ($F_{29,2}$ = 27.67, p < 0.0001; ANOVA). Rates are higher during remyelination than in healthy trained and untrained mice (p < 0.0001 and p < 0.0001, respectively; Tukey's HSD). **g, h, i**, Inter-individual variation in oligodendrocyte gain and loss is controlled for by normalizing gain to loss ("oligodendrocyte replacement"). **j,k**, Representative diagram and images of peri-electrode immunohistochemistry. Myelinated neurons within 150 microns of the electrode (indicated with white arrowhead; layer II/III XZ

maximum projection) were co-labelled with MBP (myelin; cyan), beta-IV spectrin (axon initial segment; purple) and NeuN/NFH (neuron cell soma / distal axon; green; top), whereas unmyelinated axons did not co-localize with MBP (bottom). **l**, Cuprizone administration alters peri-probe axonal myelination (Two-way ANOVA; $F_{3,8} = 110.51$, p < 0.0001). Control mice have more myelinated versus unmyelinated axons (Tukey's HSD, p < 0.0001). At the cessation of cuprizone, cuprizone-fed mice have fewer myelinated (p < 0.0001) and more unmyelinated axons than healthy controls (p < 0.0001), and more unmyelinated than myelinated axons (p = 0.004). *Note: myelin may be present elsewhere on the axon.* **m**, The proportion of unmyelinated neurons observed via IHC does not differ from the proportion of myelin loss predicted by sigmoidal demyelination characterized in Fig. 3e-h (one-sample t-test, t(2) = 1.10, p > 0.3). **p < 0.05, **p < 0.01, ***p < 0.001. Bars and errors represent Mean±SEM, points represent individual mice, for statistics see* Supplementary Table 2.3.
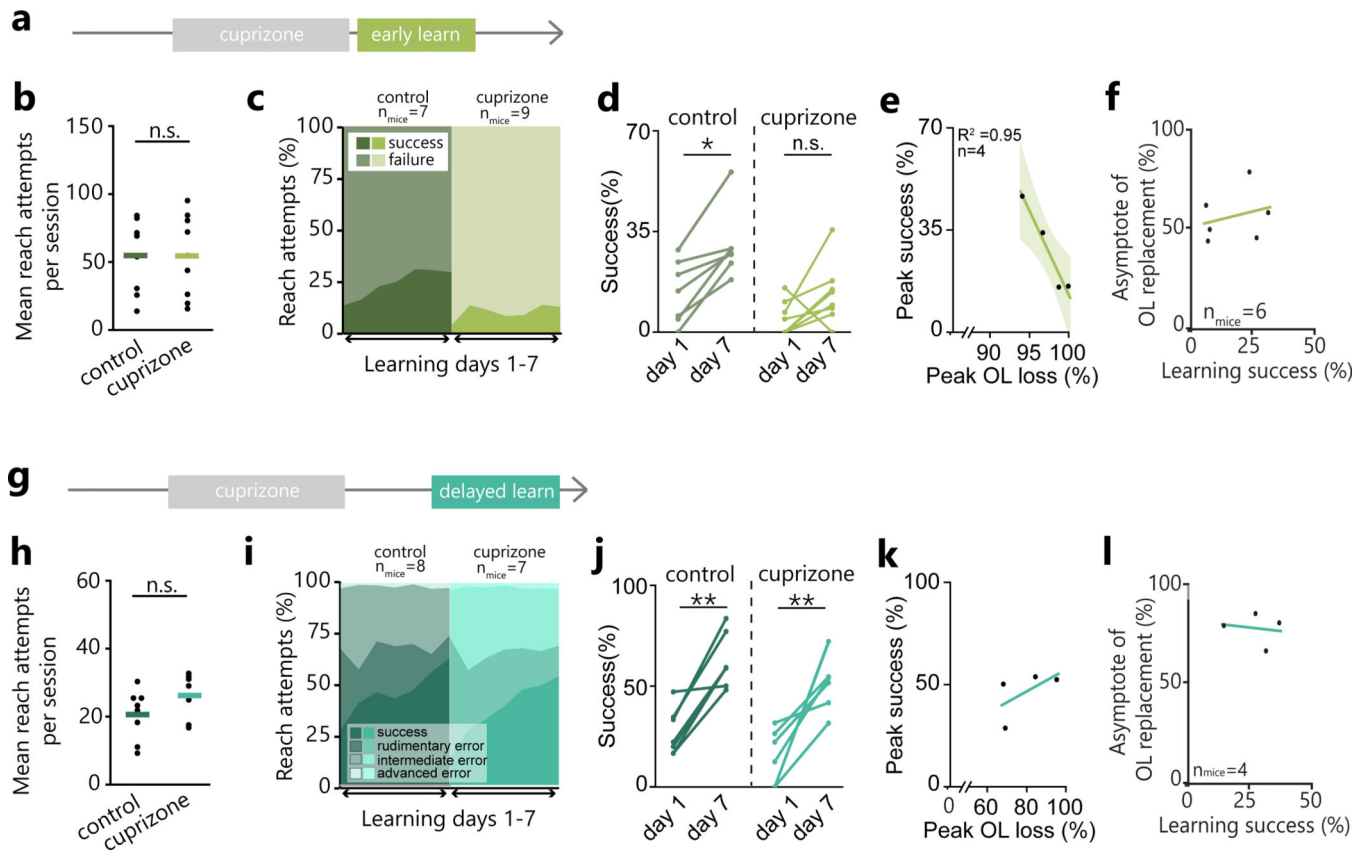
Extended Data Fig. 6: Demyelination induces deficits in early, but not delayed, motor learning.
a, Timeline for "early-learning" intervention (3 days post-cuprizone). **b**, No difference in mean reach attempts per session during early-learning between control and cuprizone-treated mice (Student's t-test, $t(12.95) = 0.05$, $p > 0.9$; coloured lines represent group means). **c**, Area plot of reach attempt outcome (success vs. failure) across forelimb reach learning days in both control and cuprizone-treated mice. **d**, Control mice have improved success rates day 7 of training relative to day 1 (Paired Student's T-test; $t(6) = 4.7$, $p = 0.003$), but cuprizone-treated mice do not ($t(7) = 1.96$, p=0.09). **e**, Maximum oligodendrocyte loss is related to peak performance during training ($R^2 = 0.95$, $p = 0.02$; line and shaded area represent line of fit and 95% confidence). **f**, No relationship between mean learning success rate (%) and asymptote of oligodendrocyte replacement in early learners. **g**, Timeline for "delayed-learning" intervention (10 days post-cuprizone) **h**, No difference in mean reach attempts per session during delayed-learning between control and cuprizone-treated mice (Student's t-test, $t(12.95) = 1.54$, $p > 0.1$; coloured lines represent group means). **i**, Area plot of reach attempt outcome (success, rudimentary error, intermediate error, advanced error; see Supplementary Video 1) across delayed-learning days in both control and cuprizone-treated mice. **j**, Both control and cuprizone-treated mice improve their reaching success between days 1 and 7 of delayed-learning (Paired student's t-test, $p = 0.0005$ and $p = 0.004$, respectively). **k**, No relationship between maximum oligodendrocyte loss and reaching performance during delayed learning. **l**, No relationship between delayed learning success rate and asymptote of oligodendrocyte replacement post-cuprizone. *$p <$
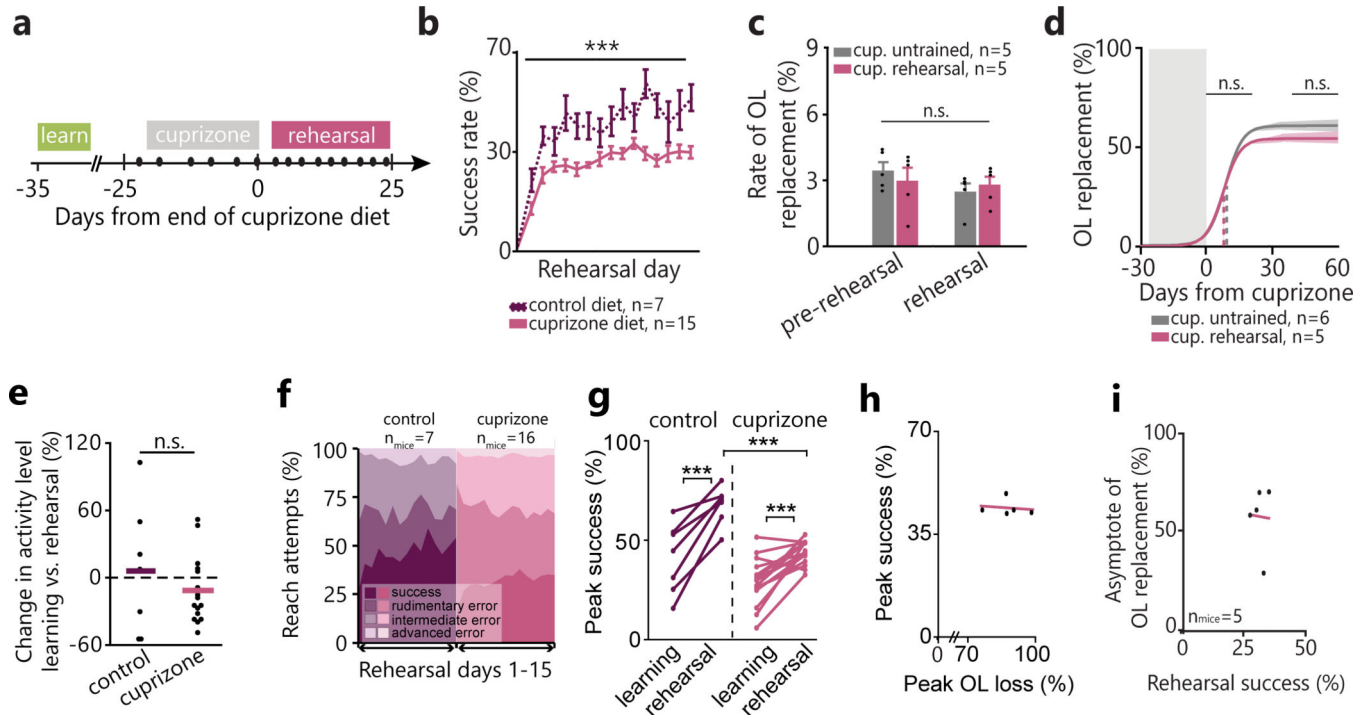
*0.05, **p < 0.01, ***p < 0.001. Points represent individual mice, for statistics see* Supplementary Table 2.5.

**Extended Data Fig. 7: Motor skill rehearsal does not modulate remyelination.**
a, Timeline of reach task rehearsal post cuprizone diet. **b,** Main effect of drug on reaching success during rehearsal ($F_{(1,14)} = 27.73$, $p < 0.0001$). **c,d,** No effect of rehearsal on rate, inflection point, or asymptote of oligodendrocyte replacement. **e,** No effect of cuprizone on change in reaching behavior between learning and rehearsal. **f,** Area plot of reach attempt outcomes in control and cuprizone-demyelinated mice. **g,** Interaction effect between performance phase (learning vs. rehearsal) and drug (control vs. cuprizone) to predict success rate ($F_{(1)} = 4.62$, $p = 0.04$). While control and cuprizone mice do not differ in success rate during pre-cuprizone learning, control mice perform significantly better during rehearsal relative to cuprizone-treated mice (Tukey's HSD, $p = 0.0004$). Both cuprizone and cuprizone-treated mice have improved performance during rehearsal relative to learning ($p = 0.0001$ and $p < 0.0001$, respectively). **h,** No relationship between peak oligodendrocyte loss post-cuprizone and peak reaching success rate during rehearsal. **i,** No relationship between rehearsal success rate and asymptote of oligodendrocyte replacement. *$p < 0.05$, **$p < 0.01$, ***$p < 0.001$. Bars and errors represent Mean±SEM, points represent individual mice, for statistics see Supplementary Table 2.5.*
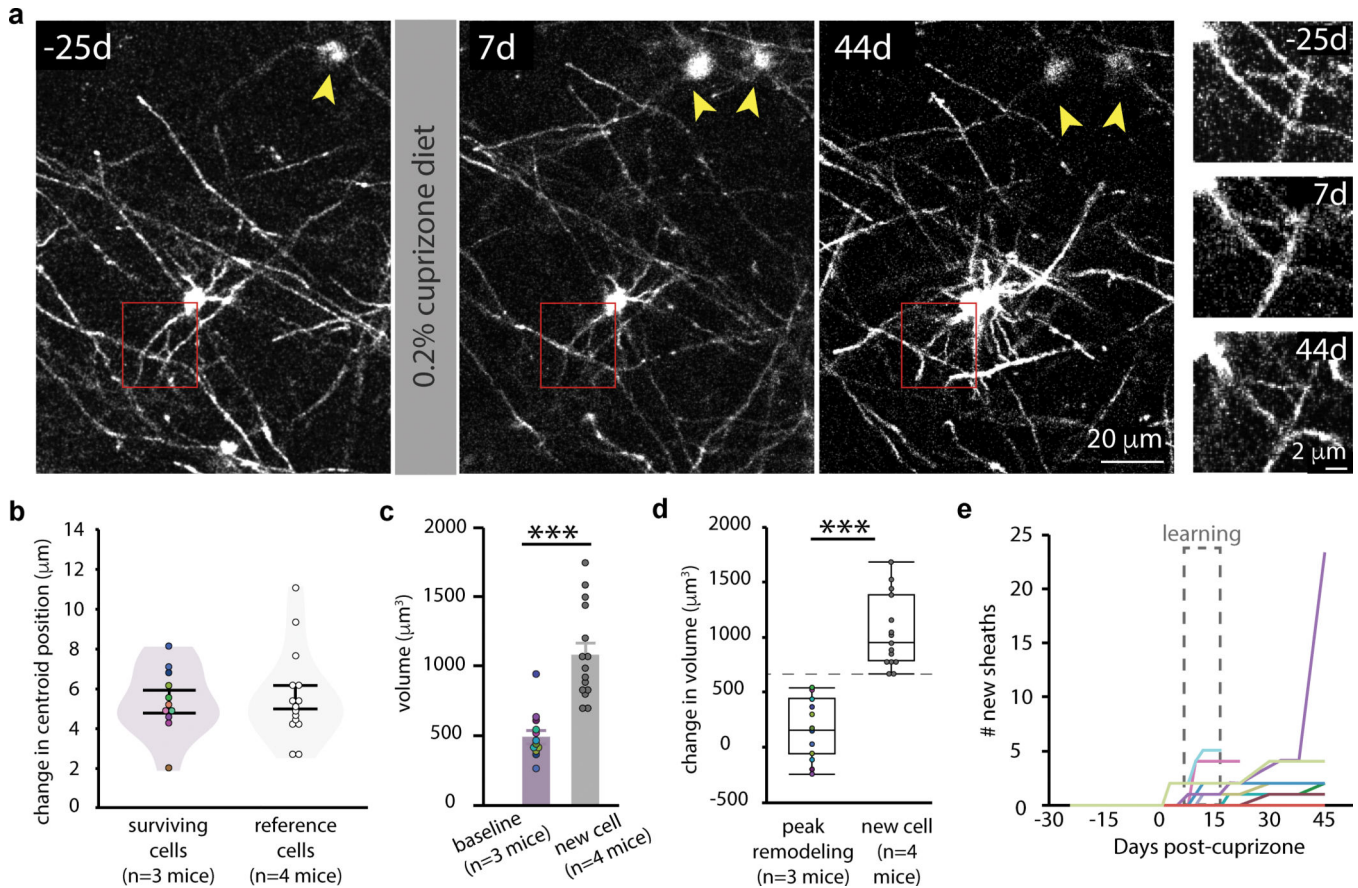
Extended Data Fig. 8: Identification of oligodendrocytes that survive demyelination.
a, Representative image outlining the methodology for following surviving oligodendrocytes over time. Single plane image of the same oligodendrocyte at baseline (−25d), one week after demyelination (7d), and six weeks after demyelination (44d). Red boxes highlight one example of the same oligodendrocyte processes lasting for the duration of the study. The maintenance of the spatial relationship between the oligodendrocyte of interest and other oligodendrocytes in the field of view (yellow arrowheads) provide further confirmation of oligodendrocyte identity. Note the new cell that appears at 7d. **b,** Change in centroid position of reference oligodendrocytes within the z-stack and surviving cell bodies from baseline to day of peak remodeling—i.e. the day where the largest number of sheaths were added by a given oligodendrocyte. **c,** Surviving oligodendrocytes at baseline are significantly smaller than new oligodendrocytes (t(21.91) = −5.81, p < 0.0001, Student's t-test). **d,** Change in volume of surviving oligodendrocytes from baseline to peak remodeling is significantly smaller than the volume of new oligodendrocytes (t(23.88 = −7.59, p < 0.0001). **e,** Dynamics of sheath addition over time. Each line represents an individual oligodendrocyte. *p < 0.05, **p < 0.01, ***p < 0.001. Bars and errors represent Mean±SEM, box plots represent Median and IQR, for statistics see Supplementary Table 2.7.
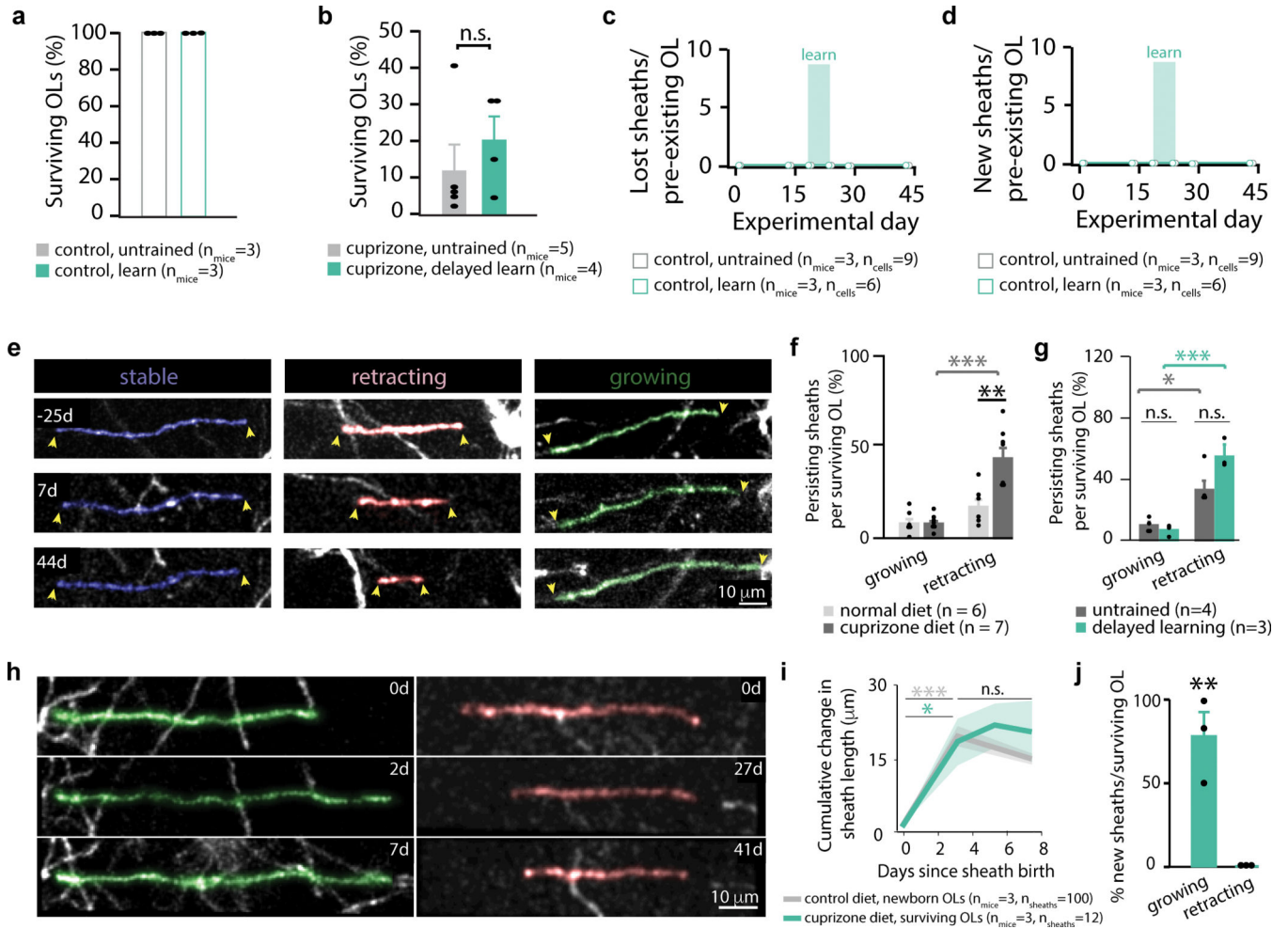
Extended Data Fig. 9: Dynamics of pre-existing and newly-generated myelin sheaths from surviving oligodendrocytes.

a, No oligodendrocytes are lost in healthy mice. **b,** No difference in percent of oligodendrocytes (OLs) surviving demyelination in untrained and delayed learning groups (Wilcoxon Rank-Sum, p > 0.5). **c, d,** No sheaths are lost (c) nor generated (d) on mature oligodendrocytes in healthy trained or untrained conditions. **e,** Behavior of pre-existing myelin sheaths that persist throughout study. Relevant sheaths are pseudo colored. **f,** Three weeks into remyelination, sheath retraction is significantly increased (F(3,22) = 18.65, p < 0.0001) when compared to age-matched controls (Tukey's HSD, p = 0.0006) and when compared to the percent of sheaths growing in cuprizone-treated mice (p < 0.0001). **g,** No effect of delayed learning on sheath dynamics during remyelination. Sheaths retract more than they grow in both untrained (p = 0.016) and delayed learning mice (p = 0.0003). **h,** Maximum projection of new sheaths generated after cuprizone exhibiting growth (pseudo colored green, left) and retraction (pseudo colored red, right). **i,** New myelin sheaths change in length in the week following their generation, whether they are from new oligodendrocytes (control: F(3,302) = 47.94, p < 0.0001) or from surviving oligodendrocytes after cuprizone-demyelination (cuprizone diet: F(3,29) = 5.31, p = 0.0049). Sheaths in both control and cuprizone treatment stabilize their length within 3 days of sheath birth (d0 vs.

d3, p < 0.0001 in control and p = 0.028 in cuprizone; Tukey's HSD). Line and shading represent mean and SEM. **j,** Sheaths from pre-existing oligodendrocytes grow more often than they retract the first three days post-generation (Wilcoxon Rank-Sum, p = 0.0029). *p < 0.05, **p < 0.01, ***p < 0.001. Bars and errors represent Mean±SEM, for statistics see Supplementary Table 2.7.
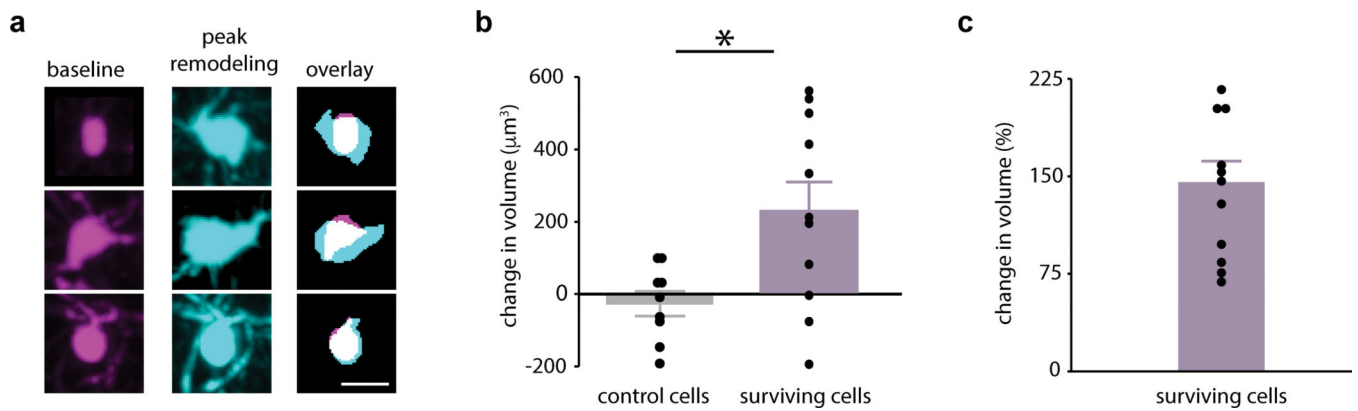
Extended Data Fig. 10: Surviving oligodendrocyte cell soma volume changes during remyelination.

a, Maximum projection of surviving oligodendrocyte cell bodies at baseline (left, magenta), peak remodeling (middle, cyan), and overlaid (right). Scale bar is 10 μm. **b,** Oligodendrocytes in normal untrained mice display little change in cell body volume throughout the study, from baseline (0d) to 43d. Surviving cells in delayed learning mice show dramatic increase in cell soma volume from baseline to day of peak remodeling when compared to oligodendrocytes in normal untrained mice ($t(12.24) = 2.56$, $p = 0.025$, Student's t-test). **c,** Percent change in volume between baseline and day of sheath addition for surviving cells engaging in remodeling. *$p < 0.05$, **$p < 0.01$, ***$p < 0.001$. Bars and errors represent Mean±SEM, for statistics see Supplementary Table 2.7.

Supplementary Material

Refer to Web version on PubMed Central for supplementary material.

Acknowledgements:

References

1. Reich DS, Lucchinetti CF & Calabresi PA Multiple Sclerosis. N. Engl. J. Med. 378, 169–180 (2018). [PubMed: 29320652]

2. Hauser SL, Chan JR & Oksenberg JR Multiple sclerosis: Prospects and promise. Ann. Neurol. 74, 317–327 (2013). [PubMed: 23955638]

3. Périer O & Grégoire A. Electron microscopic features of multiple sclerosis lesions. Brain J. Neurol. 88, 937–952 (1965).

4. Tripathi RB, Rivers LE, Young KM, Jamen F & Richardson WD NG2 Glia Generate New Oligodendrocytes But Few Astrocytes in a Murine Experimental Autoimmune Encephalomyelitis Model of Demyelinating Disease. J. Neurosci. 30, 16383–16390 (2010). [PubMed: 21123584]

5. Prineas JW & Connell F. Remyelination in multiple sclerosis. Ann. Neurol. 5, 22–31 (1979). [PubMed: 426466]

6. Green AJ et al. Clemastine fumarate as a remyelinating therapy for multiple sclerosis (ReBUILD): a randomised, controlled, double-blind, crossover trial. The Lancet 390, 2481–2489 (2017).

7. Jäkel S et al. Altered human oligodendrocyte heterogeneity in multiple sclerosis. Nature 566, 543 (2019). [PubMed: 30747918]

8. Yeung MSY et al. Dynamics of oligodendrocyte generation in multiple sclerosis. Nature 1 (2019) doi:10.1038/s41586-018-0842-3.

9. Crawford AH et al. Pre-Existing Mature Oligodendrocytes Do Not Contribute to Remyelination following Toxin-Induced Spinal Cord Demyelination. Am. J. Pathol. 186, 511–516 (2016). [PubMed: 26773350]

10. Duncan ID et al. The adult oligodendrocyte can participate in remyelination. Proc. Natl. Acad. Sci. 115, E11807–E11816 (2018).

11. Hughes EG & Appel B. The cell biology of CNS myelination. Curr. Opin. Neurobiol. 39, 93–100 (2016). [PubMed: 27152449]

12. Scholz J, Klein MC, Behrens TEJ & Johansen-Berg H. Training induces changes in white-matter architecture. Nat. Neurosci. 12, 1370–1371 (2009). [PubMed: 19820707]

13. Sampaio-Baptista C et al. Motor Skill Learning Induces Changes in White Matter Microstructure and Myelination. J. Neurosci. 33, 19499–19503 (2013). [PubMed: 24336716]

14. Beer S, Khan F & Kesselring J. Rehabilitation interventions in multiple sclerosis: an overview. J. Neurol. 259, 1994–2008 (2012). [PubMed: 22772357]

15. Albert M, Antel J, Brück W & Stadelmann C. Extensive Cortical Remyelination in Patients with Chronic Multiple Sclerosis. Brain Pathol. 17, 129–138 (2007). [PubMed: 17388943]

16. Gibson EM et al. Neuronal Activity Promotes Oligodendrogenesis and Adaptive Myelination in the Mammalian Brain. Science 344, 1252304 (2014).

17. McKenzie IA et al. Motor skill learning requires active central myelination. Science 346, 318–322 (2014). [PubMed: 25324381]

18. Xu T et al. Rapid formation and selective stabilization of synapses for enduring motor memories. Nature 462, 915–919 (2009). [PubMed: 19946267]

19. Hughes EG, Orthmann-Murphy JL, Langseth AJ & Bergles DE Myelin remodeling through experience-dependent oligodendrogenesis in the adult somatosensory cortex. Nat. Neurosci. 21, 696–706 (2018). [PubMed: 29556025]

20. Longair MH, Baker DA & Armstrong JD Simple Neurite Tracer: open source software for reconstruction, visualization and analysis of neuronal processes. Bioinformatics 27, 2453–2454 (2011). [PubMed: 21727141]

21. Harms KJ, Rioult-Pedotti MS, Carter DR & Dunaevsky A. Transient Spine Expansion and Learning-Induced Plasticity in Layer 1 Primary Motor Cortex. J. Neurosci. 28, 5686–5690 (2008). [PubMed: 18509029]

22. Hill RA, Li AM & Grutzendler J. Lifelong cortical myelin plasticity and age-related degeneration in the live mammalian brain. Nat. Neurosci. 21, 683–695 (2018). [PubMed: 29556031]

23. Hughes EG, Kang SH, Fukaya M & Bergles DE Oligodendrocyte progenitors balance growth with self-repulsion to achieve homeostasis in the adult brain. Nat. Neurosci. 16, 668–676 (2013). [PubMed: 23624515]

24. Franklin RJM & ffrench-Constant C. Regenerating CNS myelin — from mechanisms to experimental medicines. Nat. Rev. Neurosci. 18, 753–769 (2017). [PubMed: 29142295]

25. Baxi EG et al. Lineage tracing reveals dynamic changes in oligodendrocyte precursor cells following cuprizone-induced demyelination. Glia 65, 2087–2098 (2017). [PubMed: 28940645]

26. Johnson ES & Ludwin SK Evidence for a "dying-back" gliopathy in demyelinating disease. Ann. Neurol. 9, 301–305 (1981). [PubMed: 7224593]

27. Buzsáki G. Large-scale recording of neuronal ensembles. Nat. Neurosci. 7, 446–451 (2004). [PubMed: 15114356]

28. Hamada MS & Kole MHP Myelin Loss and Axonal Ion Channel Adaptations Associated with Gray Matter Neuronal Hyperexcitability. J. Neurosci. 35, 7272–7286 (2015). [PubMed: 25948275]

29. Mei F et al. Accelerated remyelination during inflammatory demyelination prevents axonal loss and improves functional recovery. eLife 5, e18246 (2016).

30. Hill RA, Patel KD, Goncalves CM, Grutzendler J & Nishiyama A. Modulation of oligodendrocyte generation during a critical temporal window after NG2 cell division. Nat. Neurosci. 17, 1518–1527 (2014). [PubMed: 25262495]

31. Picard N, Matsuzaka Y & Strick PL Extended practice of a motor skill is associated with reduced metabolic activity in M1. Nat. Neurosci. 16, 1340–1347 (2013). [PubMed: 23912947]

32. Harris JJ & Attwell D. The Energetics of CNS White Matter. J. Neurosci. 32, 356–371 (2012). [PubMed: 22219296]

33. Ortiz FC et al. Neuronal activity in vivo enhances functional myelin repair. JCI Insight (2019) doi:10.1172/jci.insight.123434.

34. Geraghty AC et al. Loss of Adaptive Myelination Contributes to Methotrexate Chemotherapy-Related Cognitive Impairment. Neuron 0, (2019).

35. Marques S et al. Oligodendrocyte heterogeneity in the mouse juvenile and adult central nervous system. Science 352, 1326–1329 (2016). [PubMed: 27284195]

36. Burke SN & Barnes CA Neural plasticity in the ageing brain. Nat. Rev. Neurosci. 7, 30–40 (2006). [PubMed: 16371948]

37. Ford MC et al. Tuning of Ranvier node and internode properties in myelinated axons to adjust action potential timing. Nat. Commun 6, 8073 (2015). [PubMed: 26305015]

38. You H et al. Aβ neurotoxicity depends on interactions between copper ions, prion protein, and N-methyl-d-aspartate receptors. Proc. Natl. Acad. Sci. 109, 1737–1742 (2012). [PubMed: 22307640]

39. Saxena S & Caroni P. Selective Neuronal Vulnerability in Neurodegenerative Diseases: from Stressor Thresholds to Degeneration. Neuron 71, 35–48 (2011). [PubMed: 21745636]

40. Witte ME et al. Calcium Influx through Plasma-Membrane Nanoruptures Drives Axon Degeneration in a Model of Multiple Sclerosis. Neuron 101, 615–624.e5 (2019). [PubMed: 30686733]

41. Werner CT, Williams CJ, Fermelia MR, Lin D-T & Li Y. Circuit Mechanisms of Neurodegenerative Diseases: A New Frontier With Miniature Fluorescence Microscopy. Front. Neurosci. 13, 1174 (2019). [PubMed: 31736701]

42. Potter LE et al. Altered excitatory-inhibitory balance within somatosensory cortex is associated with enhanced plasticity and pain sensitivity in a mouse model of multiple sclerosis. J. Neuroinflammation 13, 142 (2016). [PubMed: 27282914]

43. Van den Bos MAJ et al. Imbalance of cortical facilitatory and inhibitory circuits underlies hyperexcitability in ALS. Neurology 91, e1669–e1676 (2018). [PubMed: 30282772]

44. Kim J et al. Changes in the Excitability of Neocortical Neurons in a Mouse Model of Amyotrophic Lateral Sclerosis Are Not Specific to Corticospinal Neurons and Are Modulated by Advancing Disease. J. Neurosci. 37, 9037–9053 (2017). [PubMed: 28821643]

45. Ellwardt E et al. Maladaptive cortical hyperactivity upon recovery from experimental autoimmune encephalomyelitis. Nat. Neurosci. 21, 1392 (2018). [PubMed: 30258239]

46. Denève S & Machens CK Efficient codes and balanced networks. Nat. Neurosci. 19, 375–382 (2016). [PubMed: 26906504]

47. Hines JH, Ravanelli AM, Schwindt R, Scott EK & Appel B. Neuronal activity biases axon selection for myelination in vivo. Nat. Neurosci. 18, 683–689 (2015). [PubMed: 25849987]

48. Mensch S et al. Synaptic vesicle release regulates myelin sheath number of individual oligodendrocytes in vivo. Nat. Neurosci. 18, 628–630 (2015). [PubMed: 25849985]

49. Mori S & Leblond CP Electron microscopic identification of three classes of oligodendrocytes and a preliminary study of their proliferative activity in the corpus callosum of young rats. J. Comp. Neurol. 139, 1–29 (1970). [PubMed: 4191626]

50. Shen S, Li J & Casaccia-Bonnefil P. Histone modifications affect timing of oligodendrocyte progenitor differentiation in the developing rat brain. J. Cell Biol. 169, 577–589 (2005). [PubMed: 15897262]

Methods references

51. Schain AJ, Hill RA & Grutzendler J. Label-free in vivo imaging of myelinated axons in health and disease with spectral confocal reflectance microscopy. Nat. Med. 20, 443–449 (2014). [PubMed: 24681598]

52. Parslow A, Cardona A & Bryson-Richardson RJ Sample Drift Correction Following 4D Confocal Time-lapse Imaging. JoVE J. Vis. Exp. e51086 (2014) doi:10.3791/51086.

53. Peters A & Sethares C. Oligodendrocytes, their Progenitors and other Neuroglial Cells in the Aging Primate Cerebral Cortex. Cereb. Cortex 14, 995–1007 (2004). [PubMed: 15115733]

54. Czopka T, ffrench-Constant C & Lyons DA Individual Oligodendrocytes Have Only a Few Hours in which to Generate New Myelin Sheaths In Vivo. Dev. Cell 25, 599–609 (2013). [PubMed: 23806617]

55. Watkins TA, Emery B, Mulinyawe S & Barres BA Distinct Stages of Myelination Regulated by γ-Secretase and Astrocytes in a Rapidly Myelinating CNS Coculture System. Neuron 60, 555–569 (2008). [PubMed: 19038214]
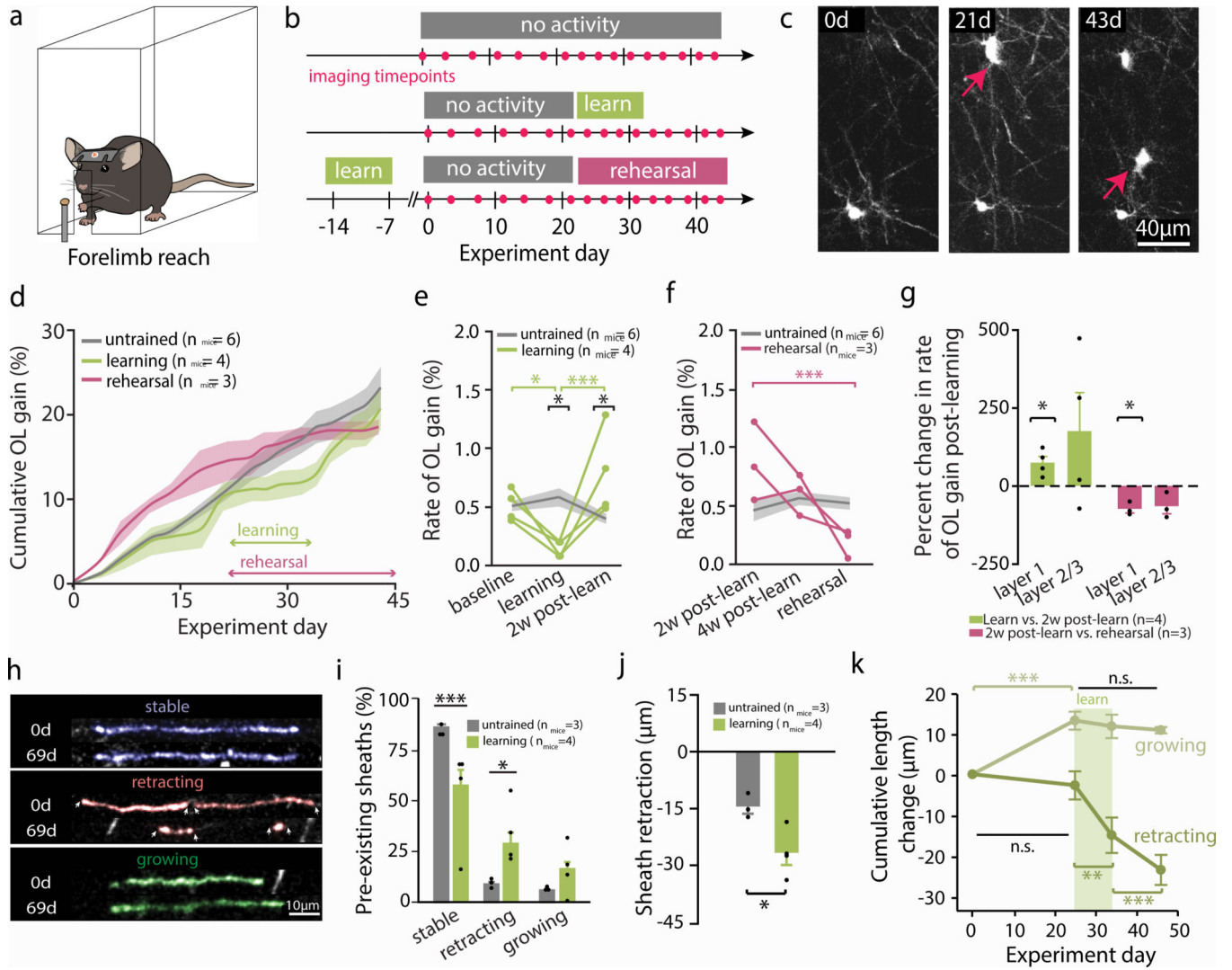
Fig. 1 |. Forelimb reach training modulates oligodendrogenesis and remodeling of pre-existing myelin sheaths.

a, b, Illustration and imaging timeline of behavioral interventions. **c**, Example of motor cortex oligodendrogenesis; red arrows indicate new cells. **d**, Cumulative oligodendrogenesis (% increase from baseline; Mean±SEM) by group. **e**, Learning modulates oligodendrogenesis rate ($F_{2,16}$=15.61, p=0.0002; grey line±shaded area represents control Mean±SEM; green traces represent individual learning mice). Rate is suppressed during learning relative to baseline (p=0.046; Tukey's HSD), resulting in a decreased rate relative to controls (p=0.016). Rate increases in the two weeks post-learning (p=0.0005; Tukey's HSD), resulting in a higher rate than controls (p=0.05). **f**, Rehearsal modulates oligodendrogenesis rate ($F_{2,14}$=10.33, p=0.002; grey line±shaded area represents control Mean±SEM; pink traces represent individual rehearsal mice). Rate decreases between two weeks post-learning and rehearsal (p=0.0009; Tukey's HSD), but does not differ between untrained and rehearsal mice. **g**, Non-zero changes in oligodendrogenesis rate (both the increase two weeks post-learning and decrease during rehearsal) are restricted to layer I of cortex (one sample t-test; p=0.037 and p=0.027, respectively; points represent individual mice). **h, i**, Learning

modulates pre-existing sheath stability (%; $F_{5,42}=69.72$, $p<0.0001$; points represent means per mouse). Learning mice have fewer stable sheaths ($p<0.0001$; Tukey's HSD) and more retracting sheaths ($p=0.014$; sheaths pseudocolored in h). **j**, Sheaths retract further in learning vs untrained mice ($n_{mice}=4$, $n_{sheaths}=59$ and $n_{mice}=3$, $n_{sheaths}=22$, respectively; Student's t-test, $t(4.62)=3.32$, $p=0.02$). **k**, "Growing" sheaths lengthen before learning (Wilcoxon Signed-Rank; $p=0.00006$) but cease growth after the onset of learning. "Retracting" sheaths are initially stable but retract during ($p=0.0047$) and after learning ($p=0.019$). *p<0.05, **p<0.01, ***p<0.001, bars and error bars represent mean±SEM. For statistics, see* Supplementary Table 2.1.
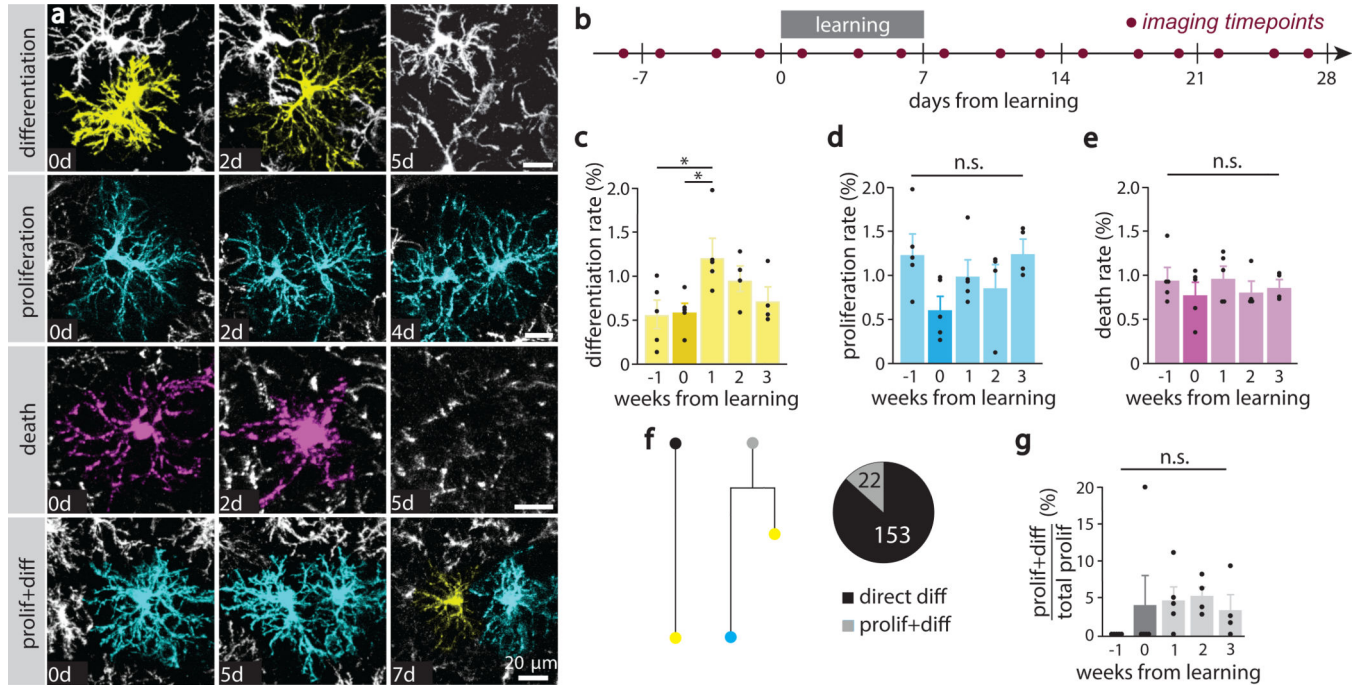
Fig. 2 |. Forelimb reach learning increases OPC differentiation.
a, *In vivo* imaging of EGFP-positive OPCs in 10 wk old *NG2-mEGFP* mice. OPCs that undergo differentiation (yellow; top) retract their filopodia, increase branching, and lose mEGFP fluorescence intensity while surrounding OPC processes infiltrate their domain. Proliferating OPCs (cyan; middle top) undergo cytokinesis and migrate to form independent domains. Dying OPCs (magenta; middle bottom) retract fragmented processes and their cell bodies become enlarged prior to disappearance. A small percentage of OPCs undergo proliferation followed by differentiation (bottom). **b**, Experimental timeline with imaging timepoints. **c**, OPC differentiation rate varies by learning week (Mean±SEM; $F_{4,14}=4.85$, $p=0.011$). Rate is increased during the first week following forelimb reach training compared to both baseline and learning week ($p=0.015$ and $p=0.021$, respectively; Tukey's HSD). **d**, No effect of learning on proliferation rate. **e**, No effect of learning on death rate. **f**, The majority (87.4%) of OPCs undergo direct differentiation (left side of cell fate diagram) as opposed to proliferation followed by differentiation (prolif+diff, right side of cell fate diagram). **g**, The proportion of differentiation events that occurred following cell division (prolif+diff) did not differ between baseline and learning or post-learning timepoints.
*$p<0.05$, **$p<0.01$, ***$p<0.001$; bars and error bars represent mean±SEM; points represent individual mice. For statistics, see* Supplementary Table 2.2.
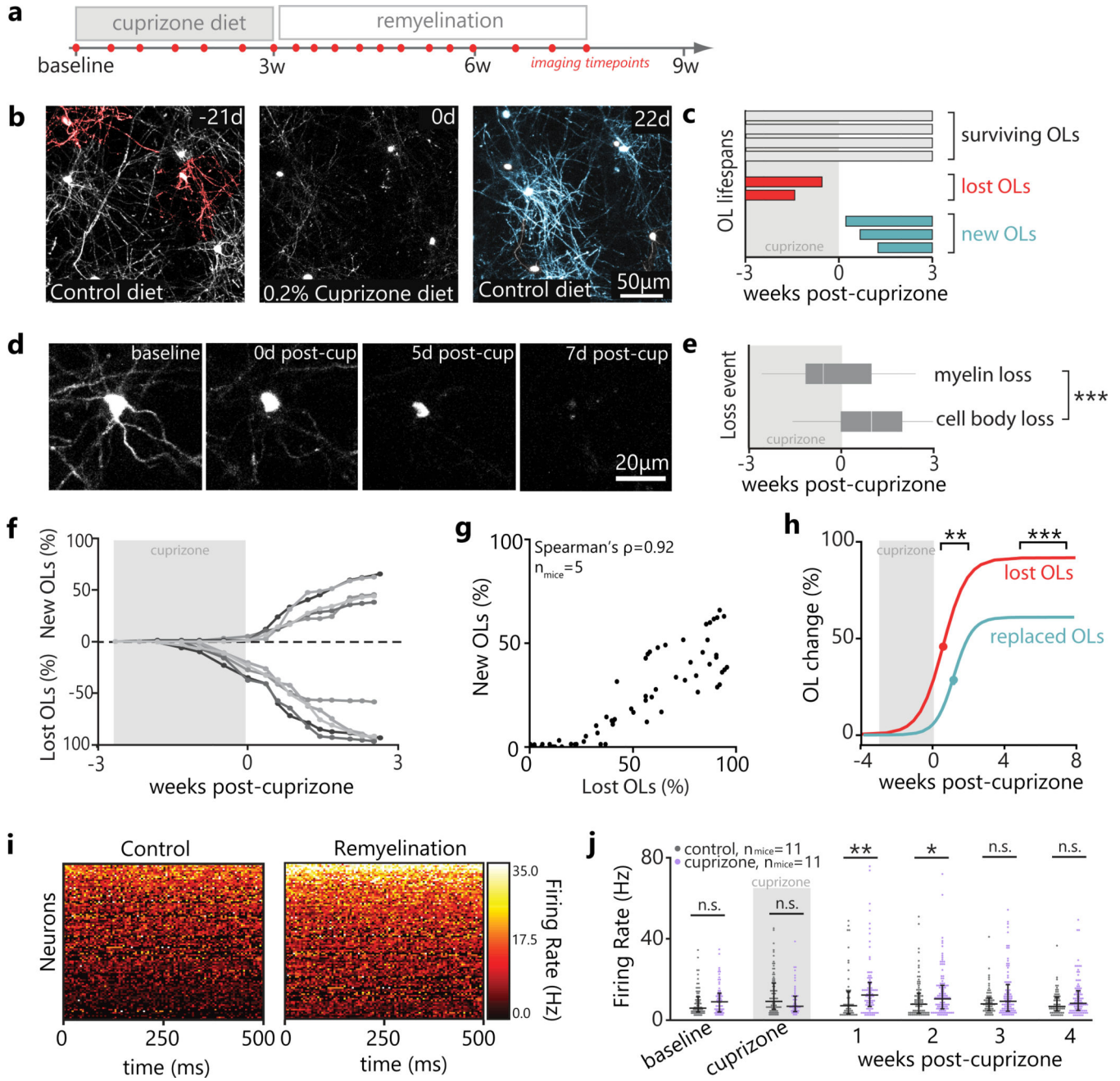
Figure 3 |. Demyelination results in incomplete oligodendrocyte replacement and functional deficits in motor cortex.

a, Timeline of cuprizone administration and *in vivo* two-photon imaging. **b, c**, Categorization of oligodendrocyte fates following cuprizone administration as "surviving" (grey), "lost" (red), and "new" (blue). Shaded area represents cuprizone administration. **d, e**, Biphasic oligodendrocyte loss: initial loss of EGFP+ myelin sheaths and subsequent shrinking of cell body before loss of EGFP signal in an *MOBP-EGFP* mouse. e, Myelin loss (n_{mice}=3, n_{cells}=45) occurs earlier than oligodendrocyte soma loss (n_{mice}=3, n_{cells}=47; Student's t-test, t(90)=−5, p<0.0001; box plots represent median and IQR). **f**, Cumulative

oligodendrocyte gain and loss relative to baseline (%); traces represent individual mice. **g**, Cumulative oligodendrocyte loss is tightly related to oligodendrocyte gain (Spearman's ρ=0.922, p <0.0001). **h**, Delayed inflection point for oligodendrocyte replacement relative to loss (8.71±0.72 vs. 4.51±0.68 days post cuprizone, respectively; n_{mice}=5; t(8)=4.24, p=0.0028; Student's t-test), and decreased asymptote of replacement relative to loss (60.52±3.03% vs. 87.06±3.10%, respectively; t(8)=6.12, p=0.0003; Student's t-test). **i**, Representative heat maps of neuronal firing rate (FR) in the motor cortex of healthy mice (left, control) versus remyelinating mice (right, cuprizone). **j**, Neuronal FR was comparable between control and cuprizone mice both prior to and during cuprizone administration, but was elevated in cuprizone mice both in the first and second week following cuprizone cessation (Wilcoxon Rank-Sum; p=0.0063 and p=0.0157, respectively; points represent individual neurons, lines and error bars represent median and IQR). By three weeks post-cuprizone, FR was indistinguishable between cuprizone and control mice. *p<0.05, **p<0.01, ***p<0.001, for statistics see Supplementary Table 2.3.
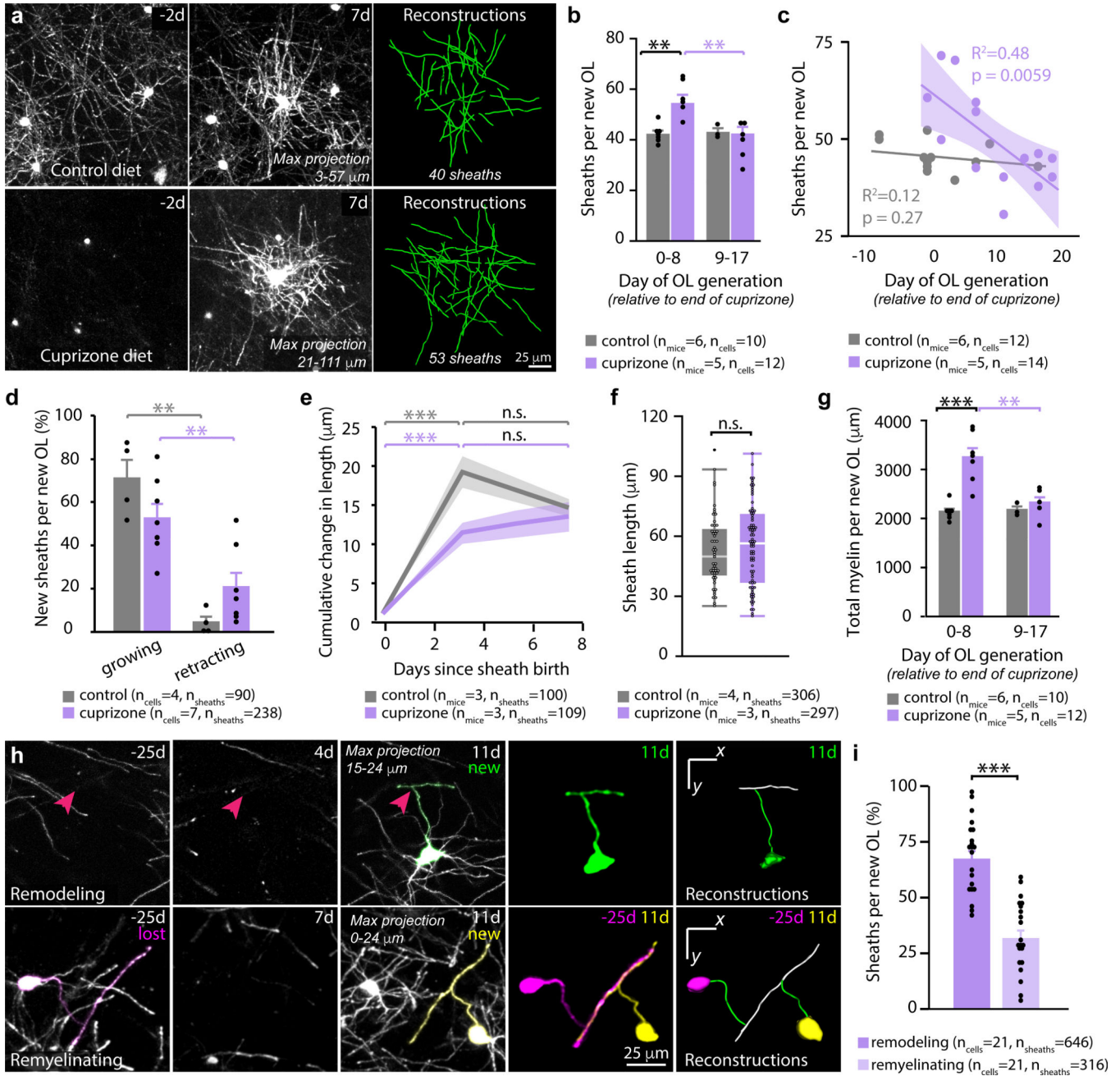
Figure 4 |. Myelin sheath number on new oligodendrocytes is regulated during remyelination.
a, b, Remyelination modulates sheath number ($F_{1,19}$=8.03, p=0.0105). Oligodendrocytes generated in the first week of remyelination (top, a) generate more sheaths than age-matched control oligodendrocytes (bottom, a; p=0.010, Tukey's HSD) or than oligodendrocytes formed after week 1 of remyelination (p=0.0023). FOV shown 2 days before oligodendrocyte birth and 7 days post-birth. Points represent individual oligodendrocytes. **c**, Day of oligodendrocyte generation relative to end of cuprizone predicts sheath number in demyelinated mice (R^2=0.48, $F_{1,12}$=11.16, p=0.006; shaded area represents 95% confidence of fit; points represent oligodendrocytes). **d**, In the first three days post-generation, sheaths

from new oligodendrocytes grow more often than they retract ($F_{3,18}$=15.34, p<0.0001) in both control (p=0.0001, n_{mice}=4) and cuprizone-treated mice (p=0.0096, n_{mice}=6, Tukey's HSD). Points represent individual oligodendrocytes. **e**, New sheaths change in length in the week following their generation (control: $F_{3,302}$=47.94, p<0.0001, cuprizone: $F_{3,293}$=29.71, p<0.0001; lines and shaded area represent mean±SEM). Sheaths in both control and cuprizone treatment stabilize their length within 3 days of sheath birth (d0 vs. d3, p<0.0001 in both treatments; Tukey's HSD). **f**, Sheath length does not differ in control and cuprizone-treated mice 3 days after sheath generation (boxplots represent median and IQR; points represent sheaths). **g**, Remyelination shapes predicted total myelin ([mean sheath length] x [# of sheaths/OL]) generated by a new oligodendrocyte ($F_{1,19}$=8.93,p=0.0077). It is higher in week 1 of remyelination than age-matched control oligodendrocytes (p<0.0001) or than oligodendrocytes generated after week 1 of remyelination (p=0.0016; Tukey's HSD). **h**, New oligodendrocytes can place sheaths in previously unmyelinated areas (top, "Remodeling") or previously myelinated areas (bottom, "Remyelinating"). Pink arrows point to location of junction between new sheath and new OL process. Relevant sheaths pseudo-colored. **i**, New oligodendrocytes engage in remodeling more often than remyelinating (t(20)=−5.08, p<0.0001,, n_{mice}=5; Paired student's t-test). *p<0.05, **p<0.01, ***p<0.001; bars and error bars represent mean±SEM, for statistics see Supplementary Table 2.4.
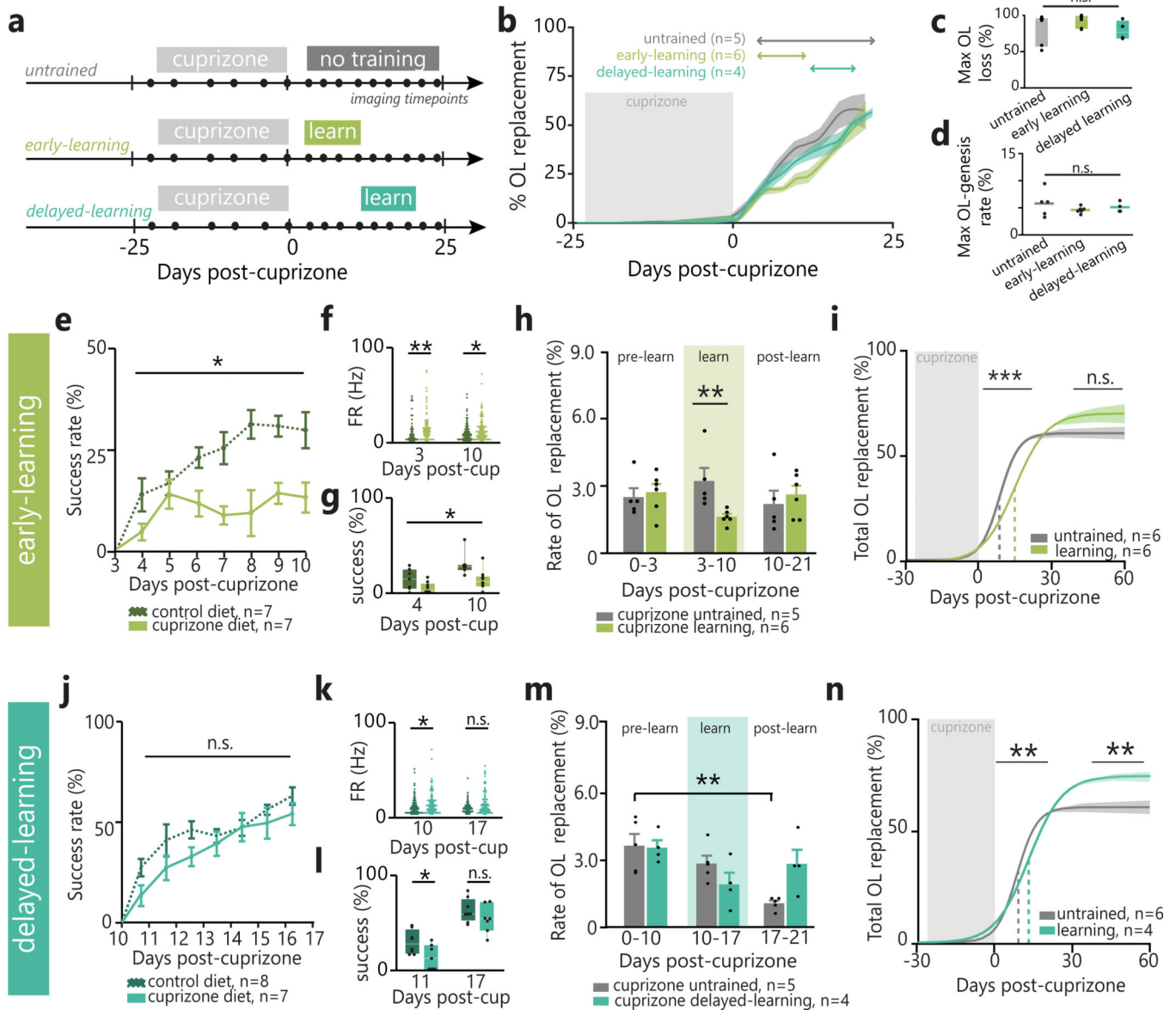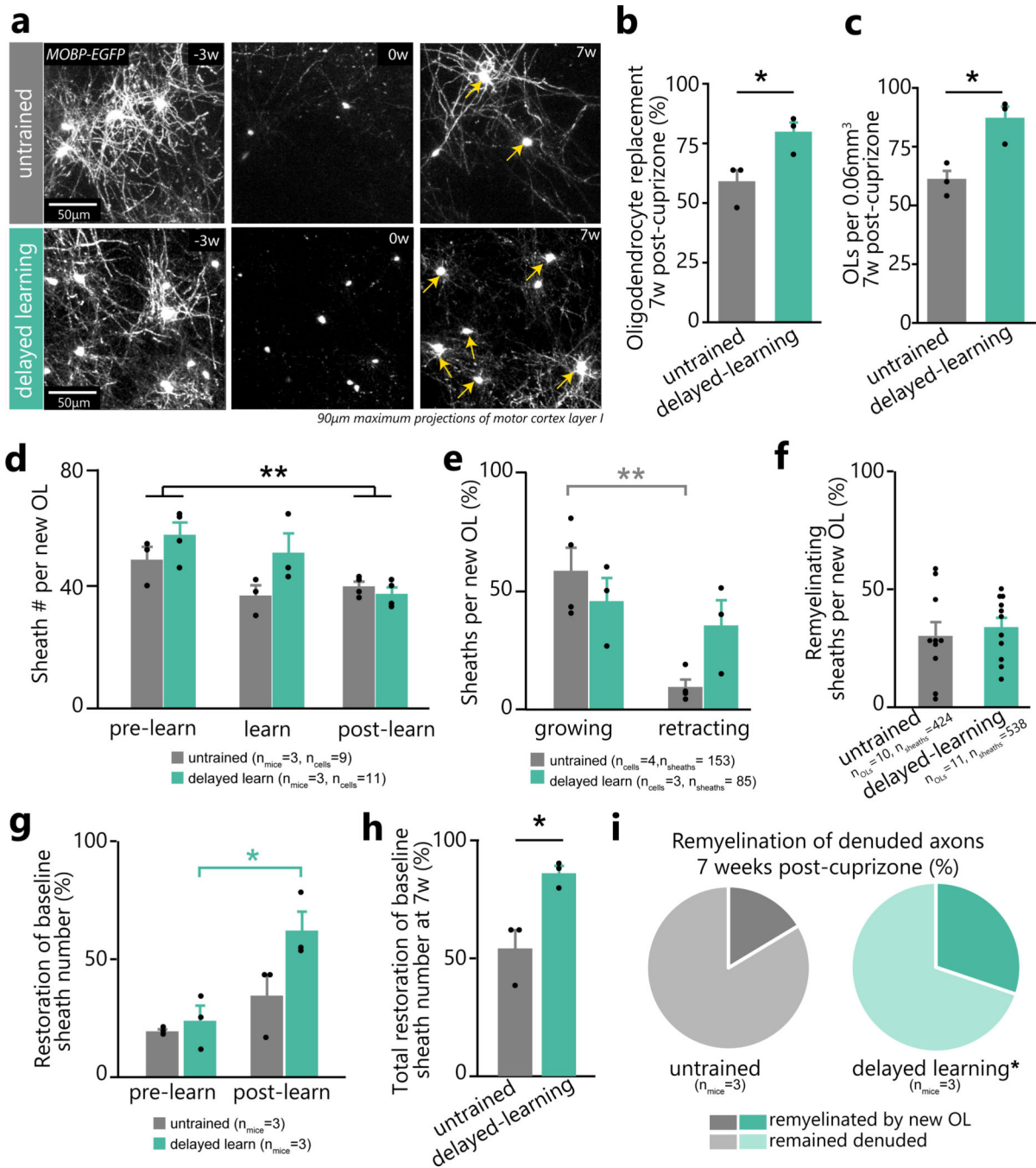
Figure 5 |. Motor learning modulates oligodendrogenesis after demyelination in a timing-dependent manner.

a,b, Cumulative OL replacement (%; lines and shaded areas represent mean±SEM) across post-cuprizone behavioral interventions. **c, d**, Neither maximum OL loss nor maximum rate of oligodendrogenesis differ between behavioral interventions (boxplots represent median and IQR). **e**, Demyelination modulates early-learning success rate ($F_{6,78}$=3.00, p=0.011, points represent mean±SEM). Success rate improves from first to last day of reaching for control (p=0.005; Tukey's HSD), but not cuprizone-treated mice. **f**, Both 3 and 10 days post-cuprizone, demyelinated mice have increased neuronal FR relative to controls (Wilcoxon Rank-Sum, p=0.006 and p=0.016, respectively; points represent neurons). **g**, Both 4d post-cuprizone and 10d post-cuprizone, demyelinated mice have decreased success rates relative to controls ($F_{1,13}$=9.09, p=0.01; points represent mice). **h**, OL replacement rate is suppressed during early-learning relative to untrained demyelinated mice (Wilcoxon Rank-Sum,

p=0.0043). i, Delayed inflection point of OL-replacement in early-learning vs. untrained demyelinated mice (Student's t-test; t(10)=5.77, p=0.0002), colored line/shaded area represents asymptote±SEM. **j**, No effect of cuprizone treatment on overall delayed-learning performance. **k**, 10 days post-cuprizone, but not 17 days post-cuprizone, demyelinated mice have increased neuronal FR relative to controls (Wilcoxon Rank-Sum, p=0.016). **l**, 11 days post-cuprizone, but not 17 days post-cuprizone, demyelinated mice have impaired reaching performance relative to controls (Student's t-test; t(12.28=−2.39, p=0.033). **m**, Delayed-learning modulates OL replacement rate ($F_{2,14}$=4.61, p=0.029). Rate decreases in untrained, but not delayed-learning, mice by 21 days post-cuprizone (p=0.008; Tukey's HSD). **n**, Delayed inflection point (Student's t-test; t(8)=4.33, p=0.0025) and increased asymptote of OL-replacement (t(8)=3.35, p=0.01) in delayed-learning vs. untrained mice. *p<0.05, **p<0.01, ***p<0.001, bars and error bars represent mean±SEM; for statistics see* Supplementary Table 2.5.

Figure 6 |. Delayed motor learning promotes remyelination via new oligodendrocytes.
a, Representative maximum-projections of superficial cortical oligodendrocytes (OLs) at baseline (left; −3 weeks), end of cuprizone diet (middle; 0 weeks), and following 7 weeks of remyelination (right) in untrained (top) and delayed-learning (bottom) mice. Yellow arrows designate new oligodendrocytes. **b, c**, Delayed-learners replace a greater proportion of lost oligodendrocytes (Student's t-test; t(3.92)=−2.99, p=0.04) and have a higher density of cortical oligodendrocytes than untrained mice (t(3.72)=−3.87, p=0.02) by 7-weeks post-cuprizone (points represent individual mice). **d**, While new OLs have increased sheath

numbers in first versus third week post-cuprizone ($F_{5,15}$=5.14, p=0.006; p=0.0038, Tukey's HSD), delayed-learning does not modulate this relationship (p=0.1; points represent individual OLs.) **e**, Delayed-learning modulates sheath dynamics ($F_{3,10}$=6.65, p=0.0095). Sheaths on new OLs are more likely to grow than retract in untrained (p=0.007, Tukey's HSD) but not delayed-learning mice (p>0.8; points represent individual OLs.) **f**, Sheaths from new OLs are equally likely to remyelinate denuded axons in untrained and delayed-learning mice (Student's t-test; t(16.08)=−0.52, p=0.6; points represent individual OLs.) **g**, Population-level extrapolations suggest that delayed-learning modulates restoration of baseline sheath number ($F_{3,8}$=7.80, p=0.0093; points represent mice). More sheaths are replaced after training in delayed-learning mice (Tukey's HSD; p=0.018). **h**, Population-level extrapolations suggest that delayed-learners restore a greater proportion of baseline sheath number 7 weeks post-cuprizone (Student's t-test; t(2.64)=−3.76, p=0.0407; points represent mice). **i**, Extrapolating sheath location probability to the population-level suggests that delayed-learners remyelinate a greater proportion of denuded axons than untrained mice (31% vs. 19%, respectively; Student's t-test; t(3.14)=−5.07, p=0.013). *p<0.05, **p<0.01, ***p<0.001, bars and error bars represent mean±SEM; for statistics see* Supplementary Table 2.6.
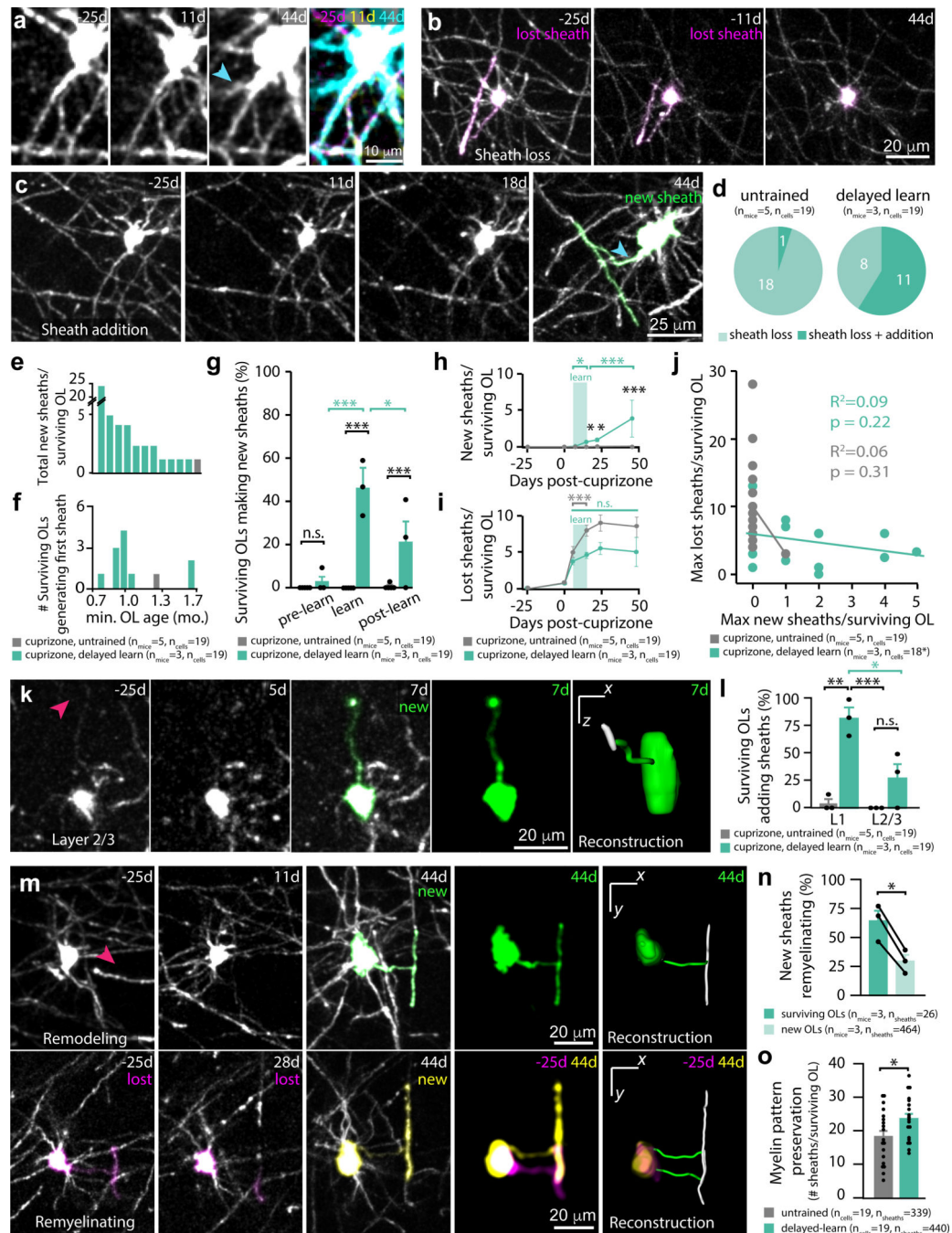
Figure 7 |. Delayed motor learning stimulates surviving mature oligodendrocytes to contribute to remyelination.

a, Identification of surviving oligodendrocytes (OLs) via conserved processes. Note the new process pointed out on the same oligodendrocyte in **a** and **c** (cyan arrow). **b,c,d**, Surviving OLs both lose (pink) and generate sheaths (green). Image manually resliced in **c** (44d) to show sheath and process connecting to cell body. **e,f**, Number of sheaths generated per surviving OL and minimum possible OL age at time of sheath generation (assuming age 0 at imaging onset). **g**, Delayed-learning modulates surviving OL sheath production ($F_{2,51}$=9.30,

p=0.0004). Sheath generation increases during learning (p<0.0001) and decreases post-learning (p=0.019), resulting in elevated generation relative to untrained mice both during (p<0.0001) and after learning (p=0.026). **h**, Learning modulates cumulative new sheaths on surviving OLs ($F_{7,618}$=12.96, p<0.0001). Delayed-learning increases new sheaths relative to baseline (p=0.019) and relative to untrained mice both during (p=0.028) and after (p=0.033) learning. Sheath number increases up to 4 weeks post-learning (p<0.0001). **i**, Learning modulates cumulative lost sheaths on surviving OLs ($F_{7,611}$=7.04, p<0.0001). Sheath loss initially increases in untrained and delayed-learning mice (p<0.0001 and p<0.0001, respectively) then ceases in delayed-learning (p>0.9) but not untrained mice (p<0.0001). **j**, No relationship between sheath loss and gain (*single outlier removed for analysis). **k,l**, Learning increases sheath generation by surviving OLs in both L1 and L/3 relative to controls ($F_{1,6}$=7.05, p=0.038; p=0.0019 and p=0.0016, respectively), though generation is heightened within L1 versus L2/3 (p=0.044). Pink arrows point to location of junction between new sheath and surviving OL process. Relevant sheaths pseudo-colored. **m,n**, Three weeks post-cuprizone, new sheaths from surviving OLs are more likely to remyelinate denuded axons than sheaths from new OLs (t(2)=7.28, p=0.018). **o**, Surviving OLs in delayed-learning mice contribute more sheaths to the original pattern of myelination (via maintenance and addition) than untrained mice (t(35)=−2.25, p=0.031). *p<0.05, **p<0.01, ***p<0.001, bars and error bars represent mean±SEM; for statistics see* Supplementary Table 2.7.